NASA/TM—2016-219002

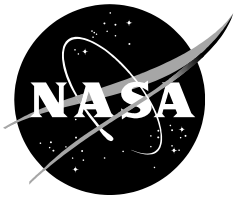

Engineering Polymer Blends for Impact Damage Mitigation

Keith L. Gordon, Russell W. Smith, Dennis C. Working, and Emilie J. Siochi
Langley Research Center, Hampton, Virginia

March 2016

NASA STI Program . . . in Profile

Since its founding, NASA has been dedicated to the advancement of aeronautics and space science. The NASA scientific and technical information (STI) program plays a key part in helping NASA maintain this important role.

The NASA STI program operates under the auspices of the Agency Chief Information Officer. It collects, organizes, provides for archiving, and disseminates NASA's STI. The NASA STI program provides access to the NTRS Registered and its public interface, the NASA Technical Reports Server, thus providing one of the largest collections of aeronautical and space science STI in the world. Results are published in both non-NASA channels and by NASA in the NASA STI Report Series, which includes the following report types:

- TECHNICAL PUBLICATION. Reports of completed research or a major significant phase of research that present the results of NASA Programs and include extensive data or theoretical analysis. Includes compilations of significant scientific and technical data and information deemed to be of continuing reference value. NASA counter-part of peer-reviewed formal professional papers but has less stringent limitations on manuscript length and extent of graphic presentations.

- TECHNICAL MEMORANDUM. Scientific and technical findings that are preliminary or of specialized interest, e.g., quick release reports, working papers, and bibliographies that contain minimal annotation. Does not contain extensive analysis.

- CONTRACTOR REPORT. Scientific and technical findings by NASA-sponsored contractors and grantees.

- CONFERENCE PUBLICATION. Collected papers from scientific and technical conferences, symposia, seminars, or other meetings sponsored or co-sponsored by NASA.

- SPECIAL PUBLICATION. Scientific, technical, or historical information from NASA programs, projects, and missions, often concerned with subjects having substantial public interest.

- TECHNICAL TRANSLATION. English-language translations of foreign scientific and technical material pertinent to NASA's mission.

Specialized services also include organizing and publishing research results, distributing specialized research announcements and feeds, providing information desk and personal search support, and enabling data exchange services.

For more information about the NASA STI program, see the following:

- Access the NASA STI program home page at http://www.sti.nasa.gov

- E-mail your question to help@sti.nasa.gov

- Phone the NASA STI Information Desk at 757-864-9658

- Write to:
  NASA STI Information Desk
  Mail Stop 148
  NASA Langley Research Center
  Hampton, VA 23681-2199

NASA/TM—2016-219002

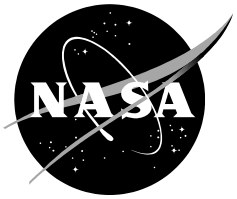

Engineering Polymer Blends for Impact Damage Mitigation

Keith L. Gordon, Russell W. Smith, Dennis C. Working, and Emile J. Siochi
Langley Research Center, Hampton, Virginia

National Aeronautics and
Space Administration

Langley Research Center
Hampton, VA 23681

March 2016

Acknowledgments

We would like to acknowledge the following colleagues for their contributions: Ms. Crystal Chamberlain for thermal analysis of polymers, Mr. Ron Penner and Mr. Richard Thomas for cutting dogbone specimens from panels, Mr. Charles Townsley for mechanical testing of specimens, Mr. Sean Britton for compression molding of polymer panels, Mr. Paul Bagby for high speed video consultation, Mr. Hoa Luong for fabrication of test frame fixture, and Mr. Brian Grimsley, Dr.(s) Godfrey Sauti, and Phillip Bogert for valuable discussions and assistance. We would also like to thank DuPont and Entec Resins for providing free samples of their respective products. We would also like to thank Dr. Marc Portanova, Mr. Donald Campbell, Mr. Joe Morrow, Mr. Ronnie Bowman, and Mr. Timothy Rouse of the Aviation Applied Technology Directorate's (AATD) Ballistic Test Range for Aircraft Component Survivability (BTRACS) facility at Ft. Eustis, VA for ballistic testing and high speed video and high speed thermal imaging recording conducted. We would also like to thank Mr. Keith Henry (INEOS) for valuable discussions and assistance involving puncture healing resin formulations.

Available from:

NASA STI Program / Mail Stop 148
NASA Langley Research Center
Hampton, VA 23681-2199
Fax: 757-864-6500

Engineering Polymer Blends for Impact Damage Mitigation

Abstract

Structures containing polymers such as DuPont's Surlyn® 8940, demonstrate puncture healing when impacted by a 9 mm projectile traveling from speeds near 300 m/sec (1,100 ft/sec) to hypervelocity impacts in the micrometeoroid velocity range of 5 km/sec (16,000 ft/sec). Surlyn® 8940 puncture heals over a temperature range of -30ºC to +70ºC and shows potential for use in pressurized vessels subject to impact damage. However, such polymers are difficult to process and limited in applicability due to their low thermal stability, poor chemical resistance and overall poor mechanical properties. In this work, several puncture healing engineered melt formulations were developed. Moldings of melt blend formulations were impacted with a 5.56 mm projectile with a nominal velocity of 945 m/sec (3,100 ft/sec) at ca. 25ºC, 50ºC and 100ºC, depending upon the specific blend being investigated. Self-healing tendencies were determined using surface vacuum pressure tests and tensile tests after penetration using tensile dog-bone specimens (ASTM D 638-10). For the characterization of tensile properties both pristine and impacted specimens were tested to obtain tensile modulus, yield stress and tensile strength, where possible. Experimental results demonstrate a range of new puncture healing blends which mitigate damage in the ballistic velocity regime.

Introduction

Among concepts under investigation for lightweight structures to meet space application requirements, is the potential of self-healing materials to enable damage tolerant, load bearing structures. Examples of areas where this class of materials may be useful are habitats and pressure vessels, including those containing propellants and other hazardous materials and especially those vulnerable to hypervelocity impacts from micrometeoroid and orbital debris (MMOD). With recent Chinese and Russian satellite detonations and collisions, the debris field orbiting Earth has become more populated, therefore, MMOD is an issue which will continue to become more critical, particularly in certain orbits.[1]

Due to its orbital location the International Space Station (ISS) is subject to numerous impacts annually. Historically, the ISS has had its MMOD systems screened in hypervelocity impact tests -- predominantly aluminum impactors, as well as some steel impaction.[2] Two protective approaches against MMOD are a metallic based Whipple Shield system (or some hybrid thereof), or multi-layered fabric based combinations for inflatable/deployable structure.[3,4] Deep Space Habitats (DSH) are projected to have much fewer MMOD hazards, with suitable protection being dictated by specific design reference missions or DRMs.

Self-healing materials display a unique ability to mitigate damage propagation, while maintaining structural load bearing capability. In recent years, researchers have studied different "self-healing mechanisms" in materials that lead to crack closure or resealing. Such approaches include:

a. crack repair in polymers using thermal and solvent processes, where the healing process is triggered with heating.[5]

b. autonomic healing, where healing is accomplished by dispersing a microencapsulated healing agent and a catalytic chemical trigger within an epoxy resin to repair or bond crack faces and mitigate further crack propagation,[6]

c. an extension of b. to the microvascular concept that utilizes brittle hollow glass tubes or fibers (in contrast to microcapsules) filled with epoxy hardener and uncured resins in alternating layers,[7-9] as an approaching crack ruptures the fluid filled glass tubes, releasing healing agent into the crack plane through capillary action. Additionally, vascular self-healing materials may also sequester the healing agent in capillary type hollow channels (Figure 1) which can be interconnected to form two dimensional and three dimensional networks.[10]

d. thermal or ultraviolet activated rebonding of a polymer (Figure 2),[11-15]

e. structurally dynamic polymers that produce macroscopic responses from a change in the materials molecular architecture without heat or pressure.[16-23]

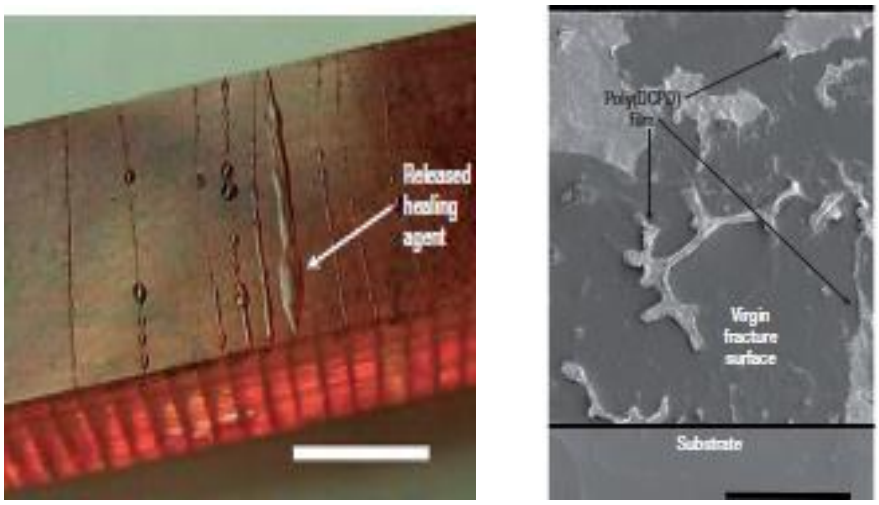

Figure 1. Self-healing microvascular networks.[10]

Although these self-healing approaches have been studied in the laboratory environment and have long been touted as having the potential to mitigate structural damage, these approaches have not been evaluated for MMOD damage mitigation under simulated operational conditions.

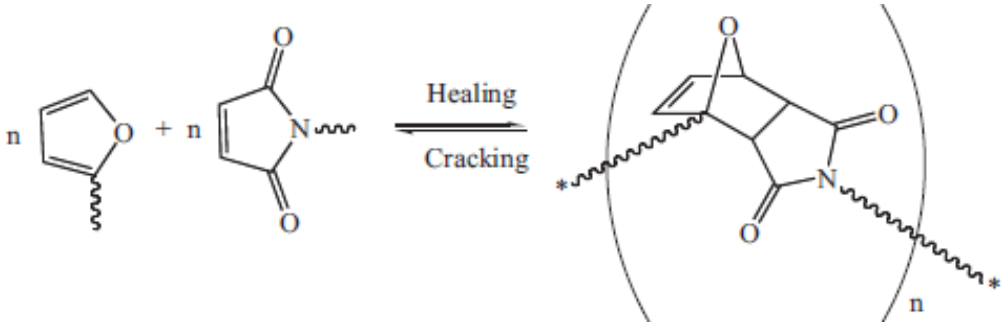

Figure 2. Self-healing Diels Alder chemistry involving Furan and Maleimides.[14]

The work reported here takes advantage of the self-healing mechanism of Surlyn® [24,25], or poly(ethylene-co-methacrylic acid) (EMMA), which flows (i.e. self-heals) following high velocity

ballistic penetration (300 m/s – 5 km/s) due to heat generated from the damage event.[26-29] Ballistic testing of Surlyn® conducted at the Langley Research Center (LaRC) suggests the healing mechanism illustrated in Figure 3. To date, a number of other commercial polymers possessing puncture healing functionality have been identified.[29,30]

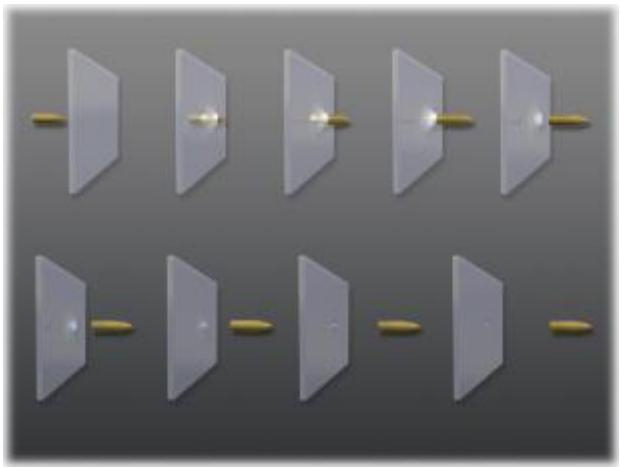

Figure 3. Projectile penetration schematic diagram.

In this work, commercially available puncture healing polymers were melt blended with engineering polymers often used for structural applications. The goal of this research was to create a suite of self-healing, structural materials with a broader range of use temperatures and survivability. Ballistic tests were used to simulate micrometeoroid damage. High speed video and high speed thermography were utilized to capture and validate the healing mechanism. Differential scanning calorimetry (DSC), and Thermogravimetric analysis (TGA) were used to assess the thermal properties of these materials. Residual structural strengths were obtained via tensile testing after impact, and residual self-healing tendencies were assessed through transverse pressure testing on impacted specimens.

Experimental

Materials

Surlyn® 8940 (Surlyn®) (DuPont) and Affinity® EG8200G (Affinity® EG2800) (Entec resins) were provided by their respective manufacturers/distributors and used as-received. LaRC phenyl ethynyl terminated imide 330 (PETI-330) (Imitec, Inc.), Bismaleimide-1 BMI-1 (Raptor Resins), Victrex poly(ether ether ketone) (PEEK), Barex® 210 IN (INEOS), Barex® 210 EG (INEOS), and Barex® 218 EG (INEOS), were purchased from their respective manufacturers and used as received. Chopped glass fibers (¼ inch/0.635 cm in length) and chopped graphite fibers (also ¼ inch/0.635 cm in length) were purchased from Fibre Glast Development Corporation. The chopped glass fibers were baked for 24 hours at ca. 560^{o}C to remove any sizing prior to use and the chopped graphite fibers were baked for 24 hours at ca. 490^{o}C to remove sizing prior to use.

Melt Processing of Puncture Healing Engineered Blends

Puncture healing melt blends were formulated by combining self-healing polymers with high performance polymeric materials. The self-healing polymeric materials consisted of Surlyn® 8940, Affinity® EG 8200G, and poly(butadiene)-graft-poly(methyl acrylate-co-acrylonitrile) (Barex®

210 IN).[30] The high performance non-self-healing polymeric materials consisted of poly(ether ether ketone) PEEK, LaRC phenyl ethynyl terminated imide 330 (PETI-330) and Raptor Resins Bismaleimide-1 (BMI-1). PETI-330 and BMI-1 are thermosets while PEEK is a thermoplastic. All of the puncture healing polymers are thermoplastics. Blends were also fabricated with chopped glass and chopped carbon fibers. The polymers were processed using a C.W. Brabender, Inc. Mixer 45/60 electrically heated with roller blades. Melt processed blends were processed at ca. 50 RPM under nitrogen purge (Figure 4).

The melt blends were prepared with two compositional variants which consisted of 95/5 and 90/10 by weight of self-healing/non-self-healing components. Melt processed blends were processed at ca. 25 rpm and at ca. 175ºC with a nitrogen gas flow of ca. 10 cc/min. The mixing temperature was selected to give the lowest viscosity at a temperature which was unlikely to cause degradation upon air exposure. Both materials were added to a funnel type weigh pan, which was then emptied into a loading hopper. Once in the mixer loading hopper, a 5 kg weight ramp was used to feed material into the mixer and nitrogen was used to continually purge the system.

Figure 4. Illustration of C.W. Brabender used to prepare melt blends.

The material was then mixed for ten minutes at ca. 175ºC. The temperature was ramped to ca. 265ºC and held for 30 minutes. If one of the materials to be blended had a higher processing or crosslinking temperature, the temperature was raised to yield a more uniform mix.

Thermal Characterization

DSC was conducted using a NETZSCH model 204-F1 Phoenix differential scanning calorimeter. Thermal scans were conducted at a rate of 20ºC/min. TGA was conducted using a NETZSCH TG-209-F1 Libra® thermogravimetric analyzer. Dynamic temperature scans were conducted at a heating rate of 5ºC/min with an initial 30 minute hold at ca. 100°C for moisture removal. TGA dynamic scans were run at temperatures ranging from ca. 25°C to 500°C.

Mechanical Testing

In order to determine the effect of healing on mechanical properties, tensile specimens were excised from impacted 3 inch by 3 inch (7.6 cm by 7.6 cm) panels (Figure 5).

(a). 5wt.% PETI330/Surlyn® proc.@ 365ºC

(b). 5wt.% PETI330/Surlyn® proc. @ 250ºC

(c). pBG/Barex® 210 IN

(d). 5wt.% BMI/Surlyn®

Figure 5. Representative 3 inch by 3 inch panels after ballistic impacts.

Where possible, three different dog-bone specimens were tested: two pristine and one impacted. The specimens were designed with ASTM D638 – 10 as a general guide (Figure 6).[31] To obtain mechanical properties, an axial-torsional Material Test System (MTS) with Skip MTS 647 hydraulic grips having diamond pattern wedges was utilized (Figure 7). MTS Flex test XE Controller with MTS Multipurpose Testware software was used to acquire data from the tests. The ramp rate in axial stroke control was 0.127 cm/min (0.050 in/min) with a continuous data sample rate of 2 Hz. Data were collected on channels which recorded time, load and stroke, as well as maximum/minimum time. Approximately 2.54 cm of the specimen was placed in the upper and lower grip wedges resulting in a specimen gage length of 2.54 cm (1 in) [i.e. the total dogbone test specimen length was 7.6 cm (3 in)].

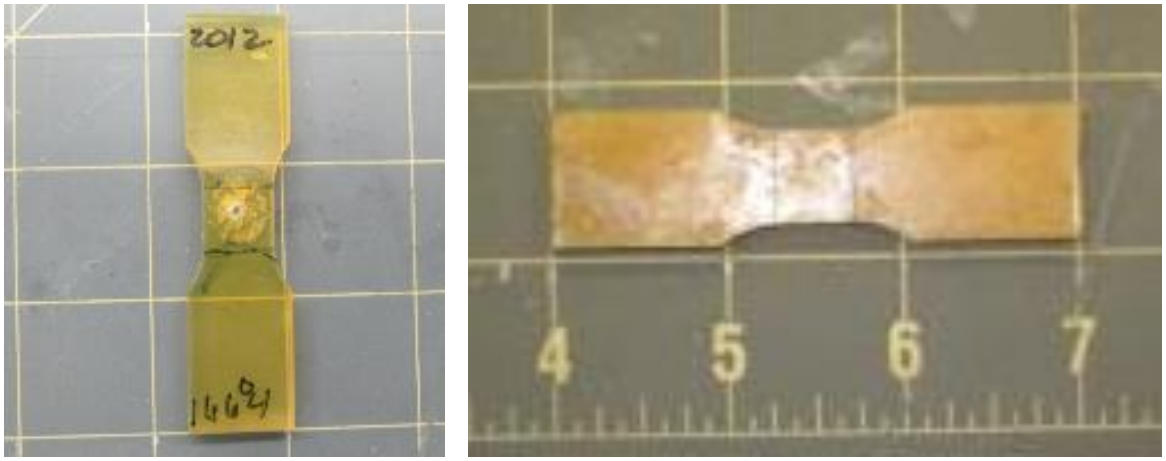

(a) impacted (b) pristine

Figure 6. Dogbone tensile test specimens.

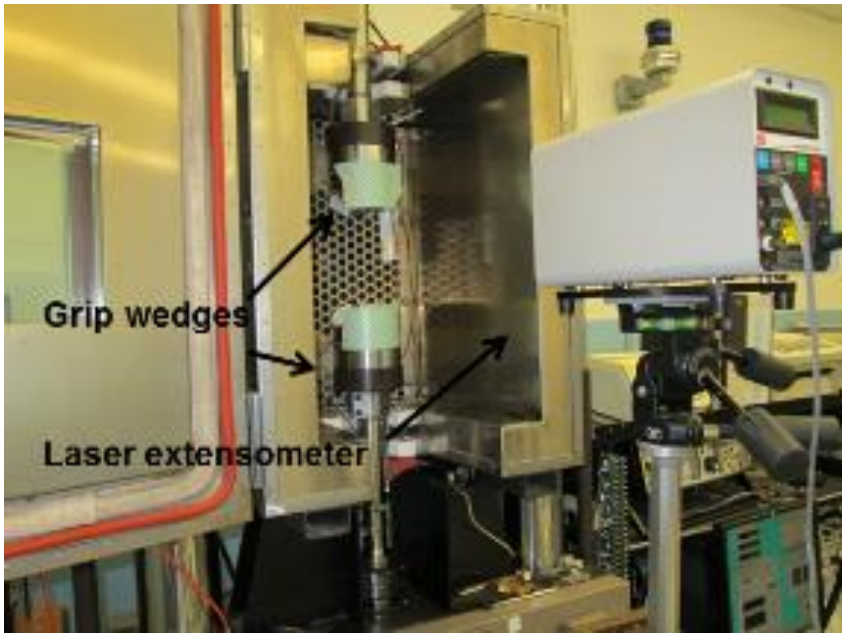

Figure 7. Axial-torsional material test system and extensometer.

Ballistic Testing

Ballistic testing was conducted to determine the self-healing characteristics of several developmental polymers subjected to low velocity penetration. To obtain dynamic damage measurements for the polymers (i.e. to simulate micrometeoroid damage), 7.6 cm x 7.6 cm x 4.9 mm thick panels were fabricated from the melt blends. These panels were impacted with a 5.56 mm x 45 NATO M193 Full Metal Jacket (FMJ), off loaded to achieve an average projectile velocity of 920 m/sec (3000 ft/sec). A ballistic "Mann" type gun mounted on a rigid frame was utilized. A laser bore sight was installed on the gun barrel to locate the ballistic impact point. A 5.56 mm x 45 barrel was used for this course of testing. Samples were evaluated at ca. 25^{o}C, 50^{o}C, and 100^{o}C. All elevated temperature tests (50^{o}C and 100^{o}C) were conducted inside an oven, and

the ballistic point of impact was captured through a glass covered door opening (Figure (s) 8 and 9). The oven allowed for variable temperature settings via a face mounted potentiometer. Temperatures of the oven chamber were monitored via a K-type thermocouple connected to a Fluke digital multi- meter. The temperature of the target was recorded with a K-type thermocouple mounted to the surface of each target and connected to a digital thermocouple meter. Two Oehler Type 57 velocity chronographs, each consisting of three infrared screens and tape readout, were placed in the shot line in front of, and behind the target, to record the pre-impact and post-impact projectile velocity. Panels were weighed before and after ballistic testing to determine material mass loss.

Figure 8. Range configuration and layout for room temperature tests.

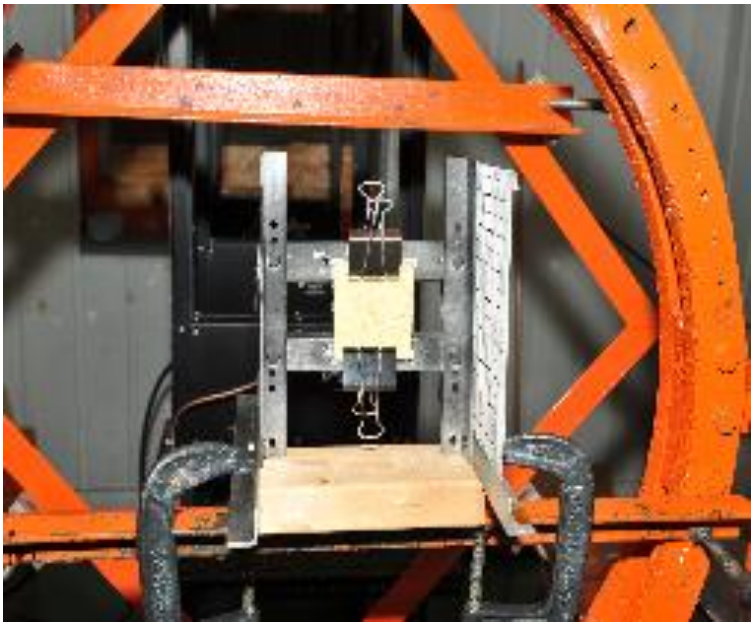

Figure 9. Test frame configuration for room temperature ballistic tests.

For the room temperature tests (25ºC), High Speed Infrared Thermography (HSIT) was utilized to determine temperature rise at the impact site. A FLIR SC6100 MWIR camera was used. It was configured to an array centered viewing resolution of 112 by 112 pixels in order to obtain a frame rate of 1804.7Hz. The l00 mm lens attached had a 7 degree field of view and a 3-5 micron band pass. In this configuration, an integration time was developed which allowed for a thermal noise floor at just below 77ºC and a saturation point just above 305°C. The infrared camera was located 2.74 meters away from the target specimen, as close to the line of fire as reasonably possible. A calibration file was taken at a similar distance and similar angle from a calibrated high temperature black body eliminating the need to apply atmospheric corrections. Recording of the tests was triggered manually to stream the data directly to disc with a lead time of ca. 3 seconds prior to weapon's firing and an approximate run time of an additional 10 seconds after impact. Post processing involved applying the calibration file and then reducing the recorded data. It is important to note that the temperature floor for the infra-red (IR) capture data is ca. 77°C. In the reduced IR data, everything below this threshold is not considered qualitative. The maximum temperature is the apparent value of the pixel with the most energy build up in the video per frame. It is not necessarily in a constant location and does not remove the possibility of hot metal or other particles (spalling, etc) in the image. Thus, all of the temperature readings are "apparent" temperatures. Specific material properties, and in particular emissivity, which changes with temperature, are required in order for actual temperature values to be calculated.

High speed video imaging utilized two Vision Research model Phantom 7.3 cameras with a frame rate of 62,000 frames per second to capture footage of the ballistics testing (Figure 10). The footage was utilized to obtain bullet velocities, rates of healing, and healing mechanisms.

Figure 10. Test configuration for elevated temperature ballistic tests.

Puncture Healing Testing

The vacuum leak method to confirm healing of puncture damage in the panels used the following procedure: a tube was connected to a vacuum pump via a fixture, such that a partial vacuum was created at the penetration location. If vacuum suction was maintained for a minimum of one hour after the vacuum pump was shut off, then panels were classified as having self-healed (Figure 11). The process was validated beforehand with non-impacted panels.

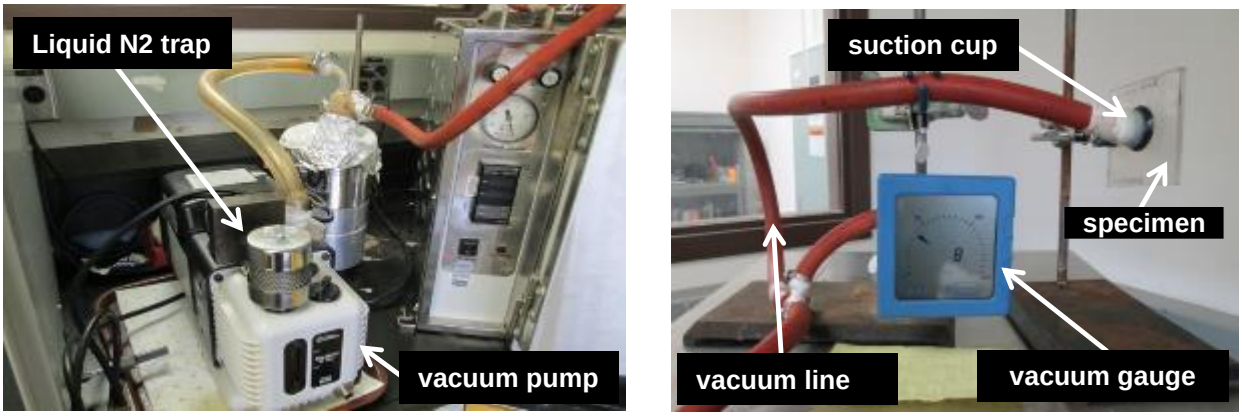

(a) Maxima C Plus, Model 4C vacuum pump (b) Surlyn® 8940 panel and vacuum gauge DVR2

Figure 11. Transverse pressure testing apparatus.

Thermal Analysis of Engineered Polymer Blends

Table 1 lists the self-healing and high performance homopolymers along with the engineered polymer blends that were prepared in these studies. Also shown are their respective glass transition temperatures (T_g), melting temperatures (T_m), and thermal decomposition temperatures. Decomposition was designated at the temperature at which a 2% or greater weight loss was reached. PETI-330, BMI-1, and PEEK are high performance polymers known for their thermal stability, with decomposition temperatures in excess of 500°C, T_g, and T_m greater than 100°C. All of the puncture healing polymers have a thermal decomposition temperature below 300°C. Both Surlyn® 8940 and Affinity® EG8200G are semi-crystalline in morphology and Barex® 210 IN is amorphous.

Resin System	Test Temp. (°C)	Site of Impact Max Temp (T) (°C)	T_g (°C)	T_m (°C)	TGA 2% Wt. Loss (°C)	Weight Loss (GN)	Hole Diameter (mm)	Self-Healing (Y or N)
Surlyn® 8940	25	240	-110	54,95	345	NA	NA	Y
Affinity® EG8200G	25	219	-68	77	288	NA	NA	Y
pBG/Barex® 210 IN	25	265	85	NA	251	NA	0.5	N
	50	265	85	NA	251	.226	NA	Y
	100	265	85	NA	251	.472	NA	Y
Barex ® 210EG	25	NA	85	NA	278	NA	1.00	N
	50	NA	85	NA	278	.370	0.94	N
	100	NA	85	NA	278	NA		Y
Barex® 218EG	25	NA	85	NA	259	NA	NA	N
	50	NA	85	NA	259	.328	NA	N
	100	NA	85	NA	259	.554	0.69	Y
PEEK	25	223	150	339	> 500	.0242	NA	N
	50	223	150	339	> 500	1.232	NA	N
	100	223	150	339	> 500	NA	NA	N
5wt.%PETI-330/ Surlyn® proc. @ 250°C	25	267	NA	93	383	056	1.21	N
	50	267	NA	93	383	.144	1.71	N
	100	267	NA	93	383	.652	.54	Y
5wt.%PETI-330/ Surlyn® proc.@ 365°C	25	255	-138	91	345	.036	1.23	N
	50	255	-138	91	345	.168	1.63	N
	100	255	-138	91	345	NA	NA	NA
10wt.%PETI-330/ Surlyn® proc. @ 250°C	25	264	-110	44, 94	372	.058	1.21	N
	50	264	-110	44, 94	372	.144	1.84	N
	100	264	-110	44, 94	372	.450	0.82	Y
10wt.%PETI-330/ Surlyn® proc. @ 365°C	25	255	NA	92	276	.036	1.47	N
	50	255	NA	92	276	.152	1.75	N
	100	255	NA	92	276	.478	0.99	Y
10wt.%PETI-330/ Affinity® EG	25	217	-57	-0.5, 62	412	.028	1.01	Y
	50	217	-57	-0.5, 62	412	.101	0.86	Y
10wt.%PEEK/Surlyn®	25	NA	-117	84, 338	379	.072	NA	N
	50	NA	-117	84, 338	379	.156	1.77	N
	100	NA	-117	84, 338	379	.214	0.98	Y
10wt.%BMI/Affinity® EG8200G	25	246	NA	65	222	.024	0.95	Y
	50	246	NA	65	222	.112	0.70	NA
5wt.%BMI/Surlyn®	25	292	-117	90	388	.074	1.48	N
	50	292	-117	90	388	.156	1.11	N
10wt.%pBG/Affinity® EG8200G	25	280	-53	64	301	.094	0.84	Y
	50	280	-53	64	301	.012	1.32	Y

Table 1. Physical Properties of Engineering Polymers and Blends.

Ballistic Testing, High Speed Thermography, and High Speed Video

High modulus polymers (PETI-330, PEEK, and BMI-1) do not demonstrate healing while lower modulus polymers (Surlyn®, Affinity® EG8200, and Barex® 210) do. Figure 12 is a thermal image of a panel immediately after impact. An increase in temperature at the impact site is observed due to frictional forces between the bullet and the material. It was observed in an earlier study that in Surlyn® 8940 and Barex® 210 IN panels, the local material at the puncture site warmed up by a measured average ΔT temperature of ca. 215ºC.[30] Self-healing in these materials is a function of the local material at the site of impact passing through thermal transitions to elevated temperature caused by impact friction. The impact temperatures in these panels are higher than the T_g and T_m for each of the polymers, thus fulfilling the requirement for the puncture event to produce a local melt state which promotes self-healing.[27]

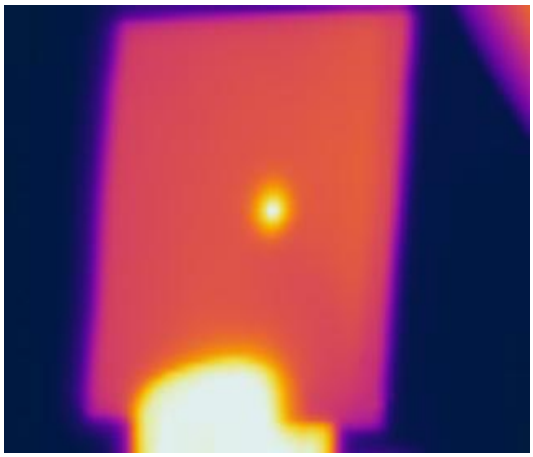

Figure 12. Thermal image of self-healing panel immediately after projectile penetration.

Table 1 lists the site of impact maximum temperatures observed in the melt blends and whether self-healing is observed; healing was observed for various blends at various temperatures. In each case where a blend was found to have healed, temperatures at the impact site were higher than the T_g's and T_m's of the respective engineered polymer blends. Elevated temperature was not the sole requirement for healing to occur. This was exemplified in polymer blends such as Surlyn® /5wt.% BMI, where the impact of temperature 292ºC was higher than both T_g and T_m, but puncture healing did not completely occur, despite the polymer blend exhibiting good impact properties. It is not surprising that this blend did not heal since BMI is a thermoset and even at the low 5% content in the blend, the cross-linked chains in the BMI was sufficient to restrict mobility or flexibility to enable hole closure. Additional energy or an increase in test temperature may be needed to permit puncture healing in the formulation. For example, Surlyn® /10wt.% PEEK did not puncture heal at ca. 25ºC or 50ºC, but did show puncture healing at ca. 100ºC. The same can be said of blends of Surlyn® /5wt.% PETI-330 and Surlyn® /10wt.% PETI-330. It is interesting to note that Affinity® appears to be more effective in enabling healing in engineering materials. This is evidenced by healing being observed in the PETI-330 and pBG compositions with Affinity®, but not in the corresponding Surlyn® blends.

Puncture healing was also observed for several Surlyn® and chopped fiber blends as shown in Table 2. The formulations were Surlyn®/5wt.% chopped glass fiber, Surlyn® /10wt.% glass fiber,

and Surlyn®/25wt.% graphite fiber. An increase in impact temperature was observed with increasing glass fiber content. Impact temperatures for the Surlyn®/5wt.% chopped glass fiber and Surlyn®/10wt.% glass fiber blends were ca. 251ºC and 264 ºC, respectively. Puncture healing was observed for both blends when shot at ca. 25ºC and 50ºC. However, a decrease of the impact temperature (188ºC) was observed for the Surlyn®/25wt.% graphite fiber blend. It is likely that the graphite fiber content in the blend increased the thermal conductivity of the blend, reducing the impact temperature. (i.e. the heat conducts more readily away from the impact location.) Nonetheless, puncture healing is observed for the Surlyn®/25wt.% graphite fiber blend when shot at ca. 25ºC.

Resin System	**Test Temp (ºC)**	**Site of Impact Max temp (T_f) (ºC)**	**Weight Loss (GN)**	**Self-Healing (Y or N)**
Surlyn® 8940	25	240	--	Y
Surlyn®/5 wt.% chopped glass fiber	25 50	251	.172 .182	Y Y
Surlyn®/10 wt.% chopped glass fiber	25 50	264	.054 .111	Y Y
Surlyn®/25 wt.% chopped graphite fiber	25 50	189	.106 .192	Y N

Table 2. Physical properties of Surlyn® 8940 and chopped fiber blends.

High speed video recording was used to capture footage of the puncture healing mechanism at the impact site during ballistics testing conducted at various temperatures. Mechanisms of self-healing have been previously confirmed and validated with high speed video for Surlyn®8940 and Barex® 210 IN panels.[30] For all of the blends, high speed video showed that the mechanism of healing observed generally followed the same healing mechanism observed for Surlyn®8940 or Barex® 210 IN.[27, 30] For the more elastomeric blends, the mechanism of healing resembled the healing mechanism observed in Surlyn®8940. For the stiff, more rigid blends, the healing mechanism more closely followed the healing mechanism of Barex® 210 IN. In the elastomeric blends, self-healing was generally observed at lower temperatures of ca. 25ºC and 50ºC. For the stiffer blends, self-healing was observed at higher temperatures due to the need for additional energy input required to initiate a viscoelastic response. For example, Surlyn®/5wt.% PETI-330 processed at 365ºC, 95%Surlyn®/5wt.% BMI, and Surlyn®/10wt.% PEEK® exhibited healing at 100ºC. However, these polymer blends did not exhibit self-healing at lower temperatures of ca. 25ºC and 50ºC. High speed video revealed that more material was lost during the impact event at the lower temperatures than at the higher temperatures. The material loss is most likely due to the glassy sample shattering at the impact site. When additional energy was provided at the higher temperature to induce chain mobility, and therefore enhanced flexibility and elasticity, the sample was better able to dissipate the energy of the bullet. This hypothesis is validated in blends such as 90% Affinity® EG8200G/10wt.% PETI330 and 95% Affinity® EG8200G/5wt.% BMI, which are more elastomeric. Healing was displayed at ca. 25ºC despite the presence of the crosslinked BMI.

Surlyn®/5wt.% chopped glass fiber, Surlyn®/10wt.% glass fiber, and Surlyn®/25wt.% graphite fiber healing mechanism resembled that of Barex® 210 IN. Addition of the chopped fibers in the Surlyn® resin matrix made the blends stiffer, thus resulting in more material loss. Despite the loss of material and the stiffness imparted by chopped fibers, healing was observed for all of the Surlyn®/chopped fiber blends.

Tensile Modulus

In order to determine the effect of healing on mechanical properties, tensile specimens were excised from the impacted 3 inch by 3 inch (7.6 cm by 7.6 cm) panels. Where possible, three different dog-bone specimens were tested: two pristine and one impacted. The specimens were designed with ASTM D638 – 10 as a general guide, but the geometry was limited due to the initial panel sizes.[31] From a structural perspective, if both the tensile modulus and tensile strength could be determined, then quantitative assessment could be rendered as to how much damage occurred during impacting, and what residual strength (or healing level) was present relative to the response of the pristine specimens. Given the small data set available, the trends outlined are qualitative, although the apparent healing tendencies for the different blends can be observed.

For systems which have a discernable yield point (the Surlyn® based blends), determination of the tensile modulus was rather straightforward and followed the ASTM standard. On the other hand, the Affinity® based blends only had a very small initial region of linearity, and hence an "initial modulus" value was calculated for comparison purposes. The Affinity® based blends also had a distinct "final modulus" curve section, which showed a substantial reduction from the initial modulus. In general, the Surlyn® blends lent themselves more towards fiber system inclusion, and the Affinity® blends more towards stand-alone self-healing layers.

The calculation of the tensile moduli was produced via a graphical method, as well as using linear regression curve fits. In essence, the initial loading versus displacement was checked for linearity, then curve fitted for stress versus strain once that load and displacement region was determined (via the mentioned linear regression, with values very close to 1.0, which would be a perfectly straight line). During the testing process, a laser extensometer was used, over a given gage length, to determine engineering stress and engineering strain. A constant cross sectional area was assumed, and hence the calculations involving the impacted specimens were of the effective modulus. It was anticipated that a tensile modulus drop-off would be apparent, as compared to the pristine specimens, but given the small sample size this proved very problematic; in determining tensile strengths, this approach again proved problematic because the specimens would run-out beyond the calibration level of the laser, and/or, the reflective gage tabs would fall off. These issues led to a less than comprehensive tensile evaluation.

In all instances where the tensile modulus is calculated, its value was the slope of the stress strain curve. In general, for the Surlyn® and Affinity® based blends, the graphical method, as detailed, led to load levels between 50 lbf – 150 lbf for the Surlyn® based tensile modulus and in the 5 lbf – 12 lbf region for the initial modulus of the Affinity® blends. However, in the case of the Affinity® blends, a final modulus load value was determined that was typically in the 32 lbf – 37 lbf loading range. The Affinity® blends retained all of their tensile strength throughout the range of deformation (i.e. the load displacement curves were essentially on top of each other, or within a very tight band), therefore, only a typical specimen was selected (generally the middle specimen response curve, regardless of whether it was impacted or pristine) to determine the tensile modulus.

Performance Properties of Engineered Polymer Blends: Residual Strength and Tensile Properties

To further quantify self-healing tendencies, residual strength tests were conducted for both pristine and post-impacted specimens. Tensile strengths were calculated using maximum load force values obtained prior to failure for the engineered polymer blends. Results for puncture healing blends are plotted in Figure(s) 13-36. Maximum load, at ultimate tensile strength, were recorded for both pristine and impacted blends and used in residual strength calculations. Self-healing was also validated by a secondary vacuum leak test method. Shown in Table 3 is a listing of the puncture healing melt blend tension after penetration (TAP) residual strengths and pressure testing results.

Polymer Blends[a]	**Test Temp (°C)**	**TAP Retention [b] (%)**	**Vacuum Hold Time [c] (mins.)**	**Projectile Penetration Diameter (mm)**
Surlyn®/5wt.%PETI330 proc. @ 250°C	100	80	60	0.54
Surlyn®/10wt.%PETI330 proc. @ 250°C	100	72	60	0.82
Surlyn®/10wt.%PETI330 proc.@ 365°C	100	73	60	0.99
Surlyn®/5 wt.% chopped glass fiber	25 50	74 69	60 60	1.43 NA
Surlyn®/10 wt.% chopped glass fiber	25 50	83 78	60 60	1.49 1.60
Surlyn®/25 wt%. chopped graphite fiber	25	56	60	1.50
Surlyn®/5wt.%BMI	100	83	60	0.48
Affinity® EG8200G/10wt.%PETI330	25	100	60	1.01
Affinity® EG8200G/5wt.% BMI	25 50	100 97	60 60	0.95 0.89
Affinity® EG8200G/5wt.% Barex® 210 IN	25 50	100 99	60 43	1.02 0.94
Affinity® EG8200G/10wt.% Barex® 210 IN	25 50	97 98	60 30	0.84 1.32

a - wt.%
b - retention of baseline strength
c - vacuum test suspended after 60 mins.

Table 3. Tension After through Penetration (TAP) and Vacuum Hold Times of Engineered Blends

Tensile Modulus

As can be seen in Figure 13, tensile strengths for both the impacted and pristine specimens, continued past the initial yield point, but in the case of specimen #2, which was pristine, it failed prior to maximum stroke as compared to specimen #1. This tends to indicate damage occurred in what was believed to be a pristine specimen and was a result of attempting to get three specimens from each fabricated panel. Figure 14 shows very consistent modulus values and due to the increase in the test temperature, at which ballistic testing was conducted, both healing and modulus values were enhanced. It should also be noted, that in general, and where applicable, both load vs. displacement data plots were generated for a specimen set, along with tensile modulus values. Within any given tensile modulus plot, the slope of the root mean square (rms) curve fit is the slope of the stress vs. strain curve (i.e. the constant which multiples the x variable) and the quality of the curve fit is denoted by the residual error term, or R^2, within any given plot.

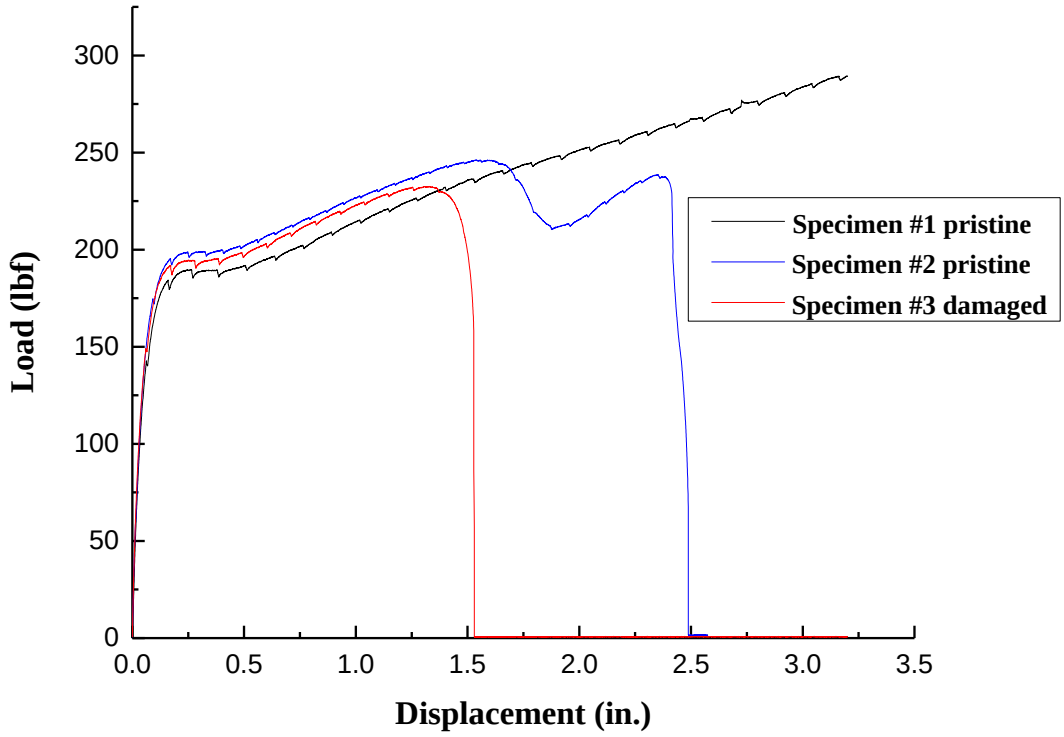

Figure 13. Load displacement curves for non-impacted and impacted Surlyn®/5wt.% PETI-330 processed at 250°C blends (shot at 100°C).

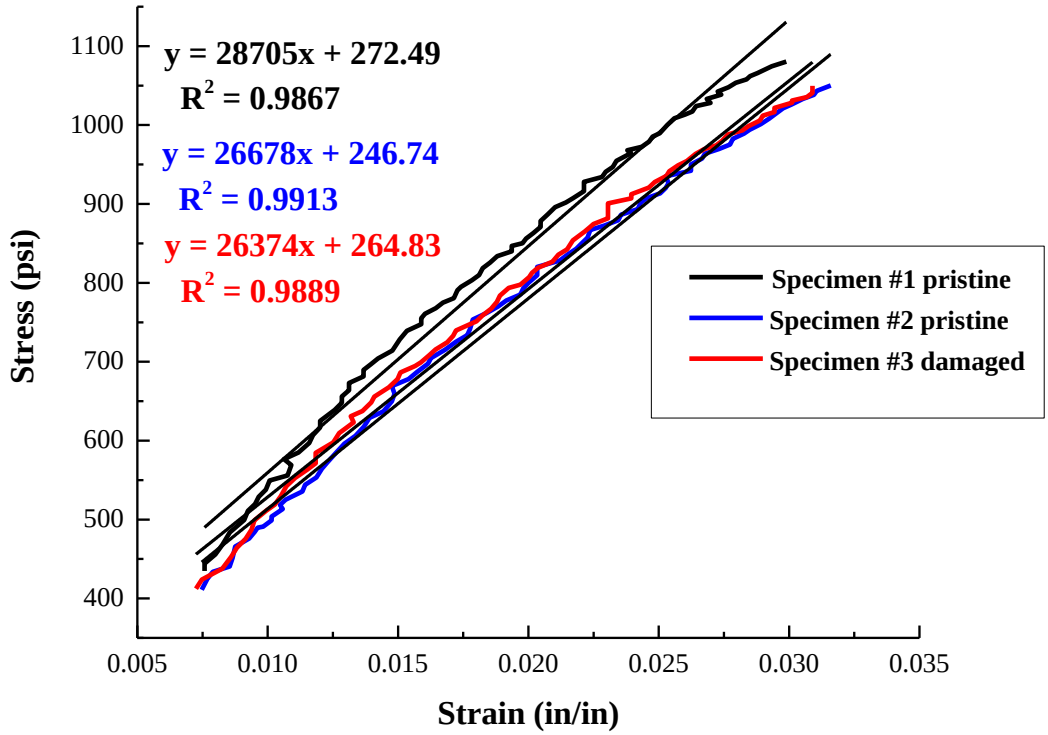

Figure 14. Tensile modulus for Surlyn®/5wt.% PETI-330 (shot at 100ºC).

Utilizing the load vs. displacement curve as shown in Figure 15, it can be seen that the impacted specimen retained about 165 lbf /225 lbf, or, about 73% of its tensile strength over the range of deformation; the tensile modulus calculations for the same specimens are shown in Figure 16. Over the initial linear range for both specimens, a fairly uniform modulus value was calculated. Two pristine specimens could not be fabricated for this test due to un-symmetric damage away from the middle of the original, impacted, 3 inch by 3 inch fabricated panel.

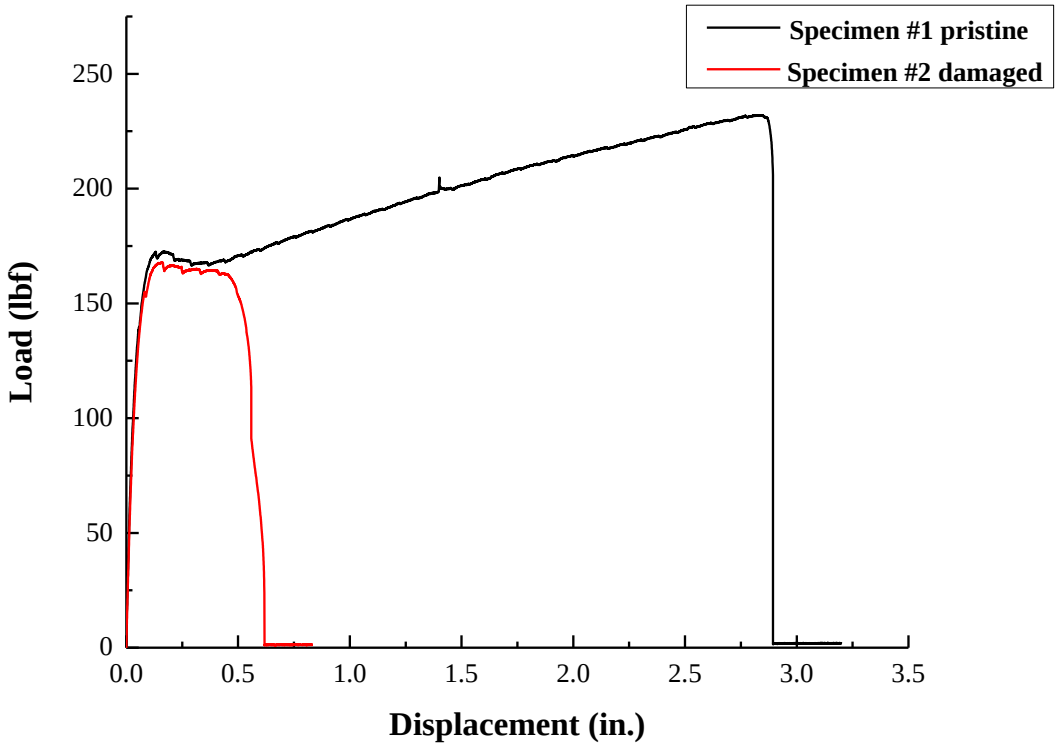

Figure 15. Load displacement curves for non-impacted and impacted Surlyn®/10wt.% PETI-330 processed at 365ºC (shot at 100ºC) blends.

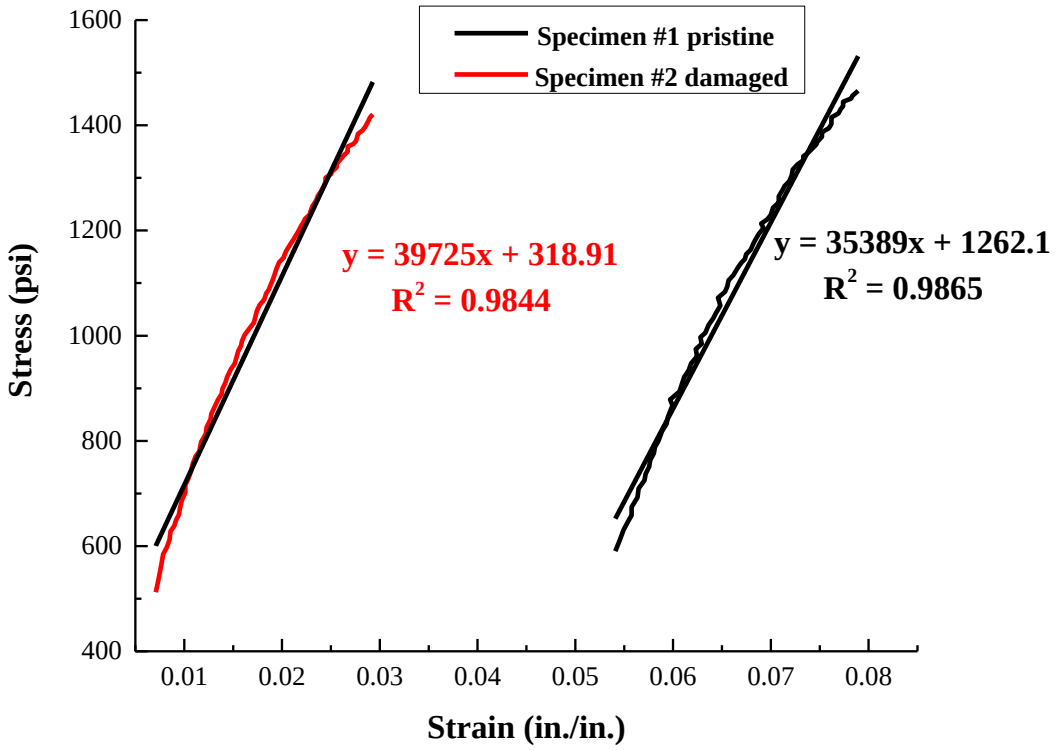

Figure 16. Tensile modulus for Surlyn®/10wt.% PETI-330 (shot at 100ºC).

Shown in Figure 17, the yield load of the impacted specimen is greater than that of the second pristine specimen, which tends to indicate some degree of damage in pristine specimen #2; modulus calculations for the same specimens are shown in Figure 18. However, specimen #1 had a substantially greater modulus, which is not well understood at this point, and requires greater in depth investigation to diagnose precisely; it is indicative that there was actual damage in the pristine specimen #2.

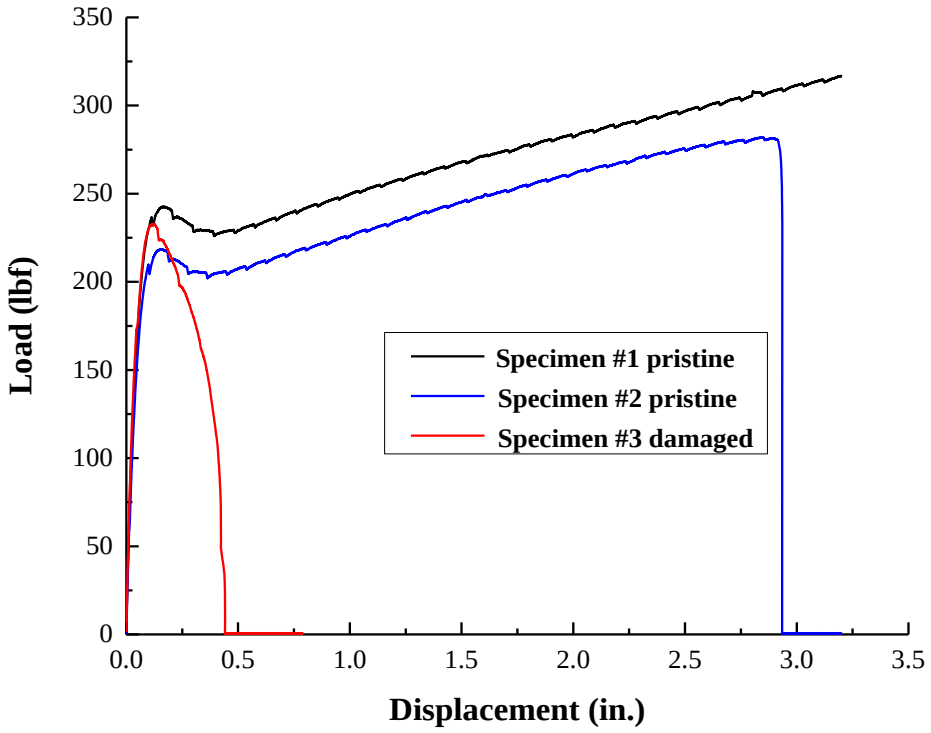

Figure 17. Load displacement curves for non-impacted and impacted Surlyn®/5wt.% BMI (shot at 100ºC).

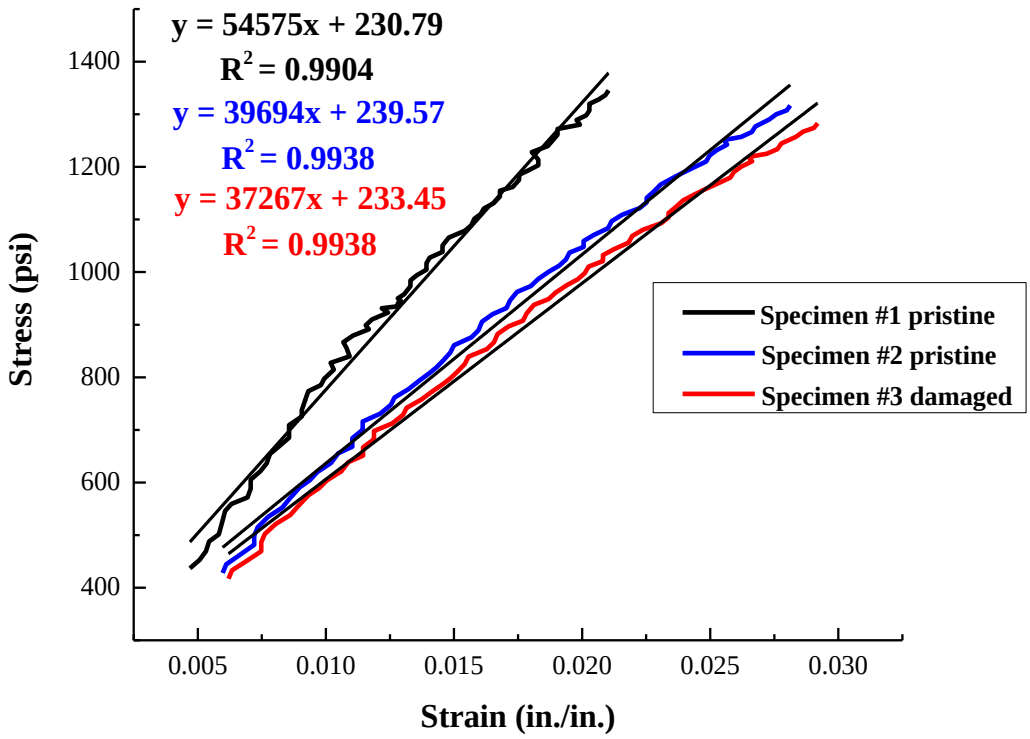

Figure 18. Tensile modulus for Surlyn®/5wt.% BMI blends at 100ºC.

Shown in Figure 19 is the Surlyn®/5wt.% chopped glass fiber blends which were shot at 25ºC and at 50ºC. Due to a laser extensometer tab issue, the modulus of the first pristine specimen could not be captured at 25ºC. At elevated ballistic test temperatures of 50ºC, the specimen shows a greater deformation and a reduction in material properties, stiffness and yield load.

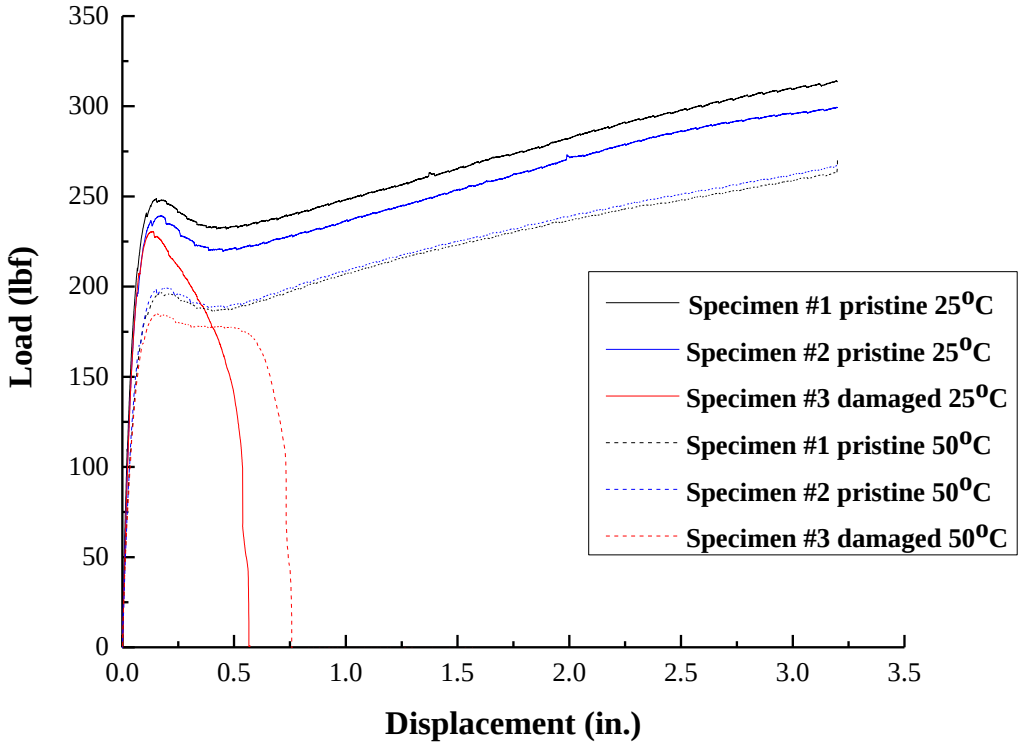

Figure 19. Load displacement curves for non-impacted and impacted Surlyn®/5wt.% chopped glass fiber blends (shot at 25°C and 50°C).

The tensile modulus values shown in both Figure 20 and 21 were determined in an identical fashion. Linearity of the load vs. displacement response was affirmed, and those same loading levels were used for the modulus calculation. It should be noted that this is the same data reduction method utilized for all tensile modulus calculations, based upon the linear curve fit of the load vs. displacement response, per given specimen(s).

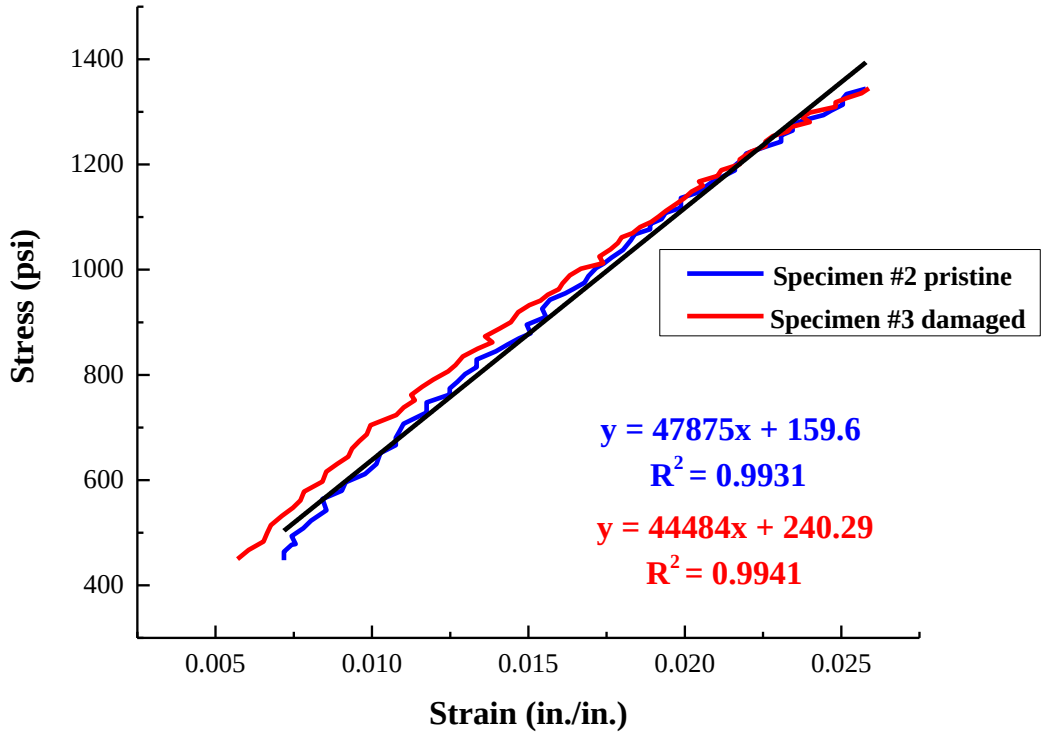

Figure 20. Tensile modulus for Surlyn®/5wt.% chopped glass fiber blends (shot at 25ºC).

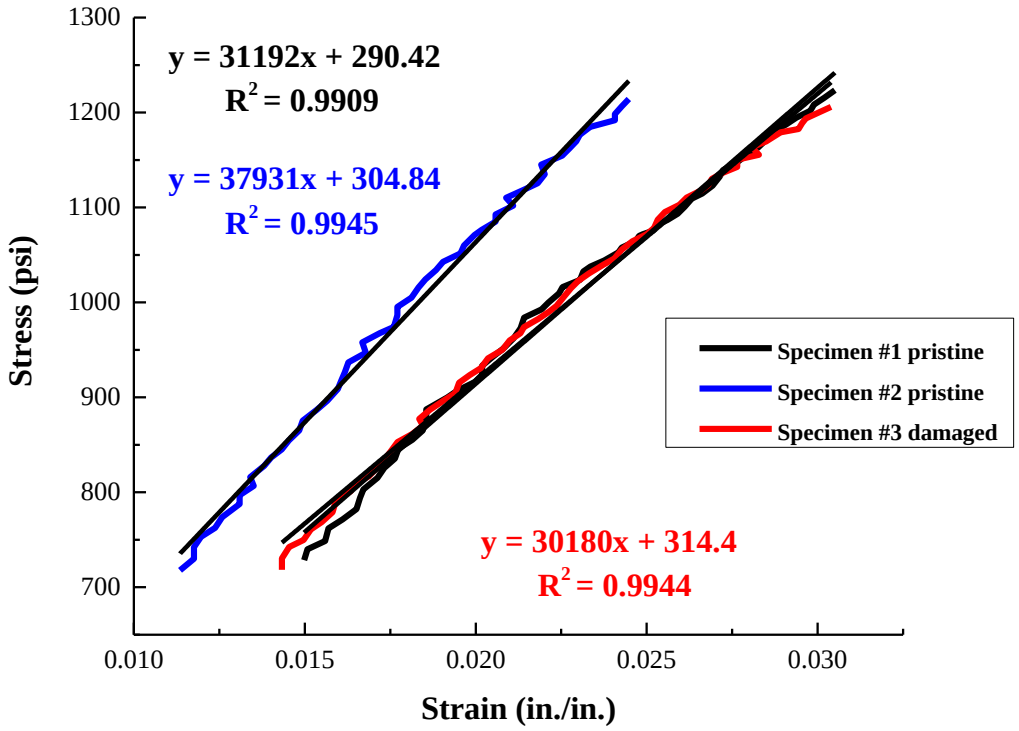

Figure 21. Tensile modulus for Surlyn®/5wt.% chopped glass fiber blends (shot at 50°C).

The Surlyn® blend with 10wt.% chopped glass fibers, impacted at 25°C and 50°C, respectively, are shown in Figure 22 for load vs. displacement; tensile modulus values for this blend were fairly consistent as shown in Figures 23 and 24. However, for the specimen #1 tensile modulus as shown in Figure 23, the laser extensometer dropped off early in the test sequence, and hence a higher value was calculated as compared to the other tested specimens. Additionally, in the load vs. displacement response the impacted specimen #3 failed shortly after yielding for both temperature cases. Additionally, both of the pristine specimens for this set (25°C) showed tensile strength load values of between 240 lbf - 270 lbf (i.e. tensile strengths = 2,672 psi and 3,034 psi, respectively; with an average tensile strength = 2,853 psi). Thus, it can be noted that the impacted specimen retained around 83% of its residual tensile load (and hence strength). For the 50°C specimen set, the residual strengths can be seen to be about 78% based upon the load vs. displacement data.

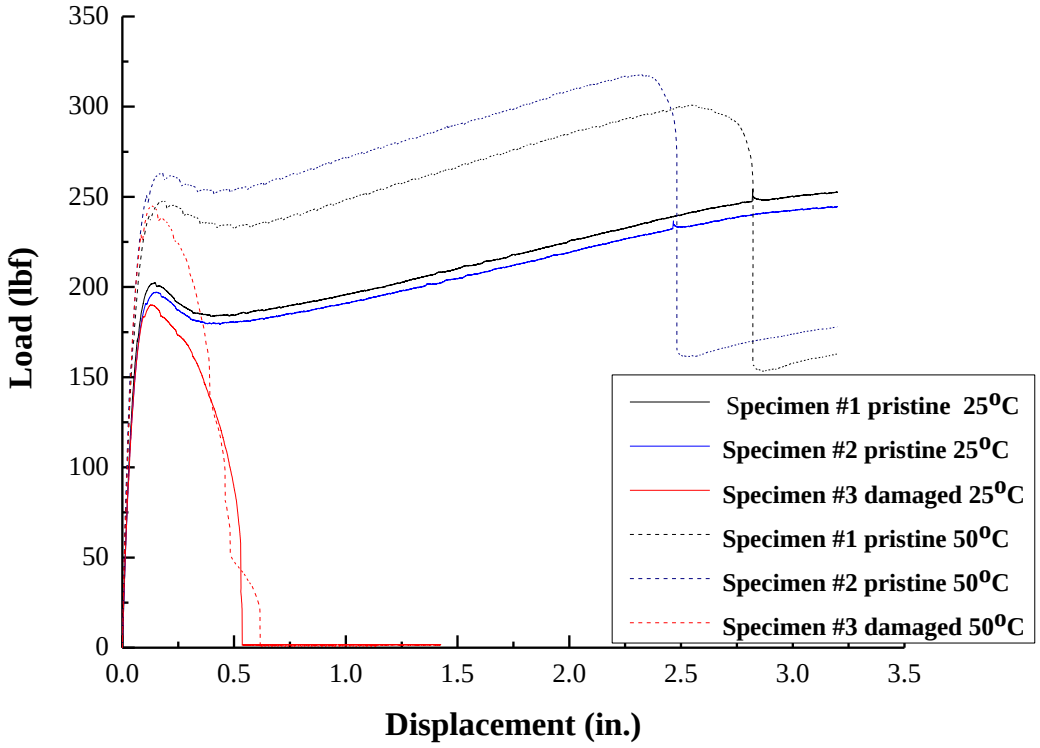

Figure 22. Load displacement curves for non-impacted and impacted Surlyn®/10wt.% chopped glass fiber blends (shot at 25ºC and 50ºC).

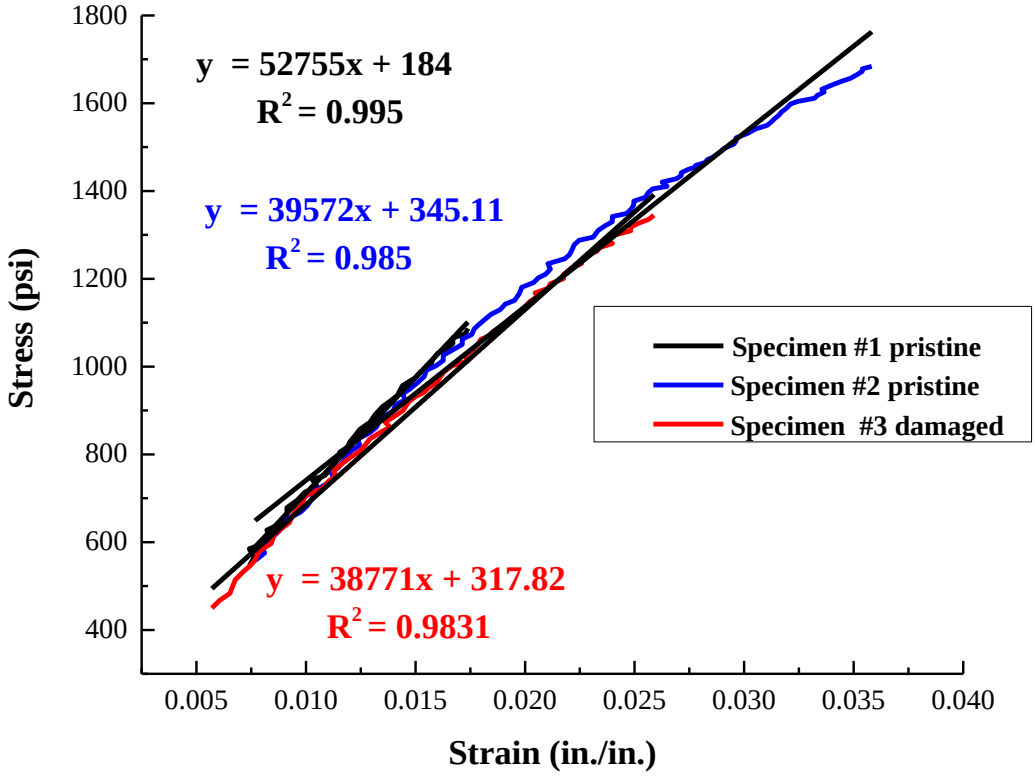

Figure 23. Tensile modulus for Surlyn®/10wt.% chopped glass fiber blends (shot at 25°C).

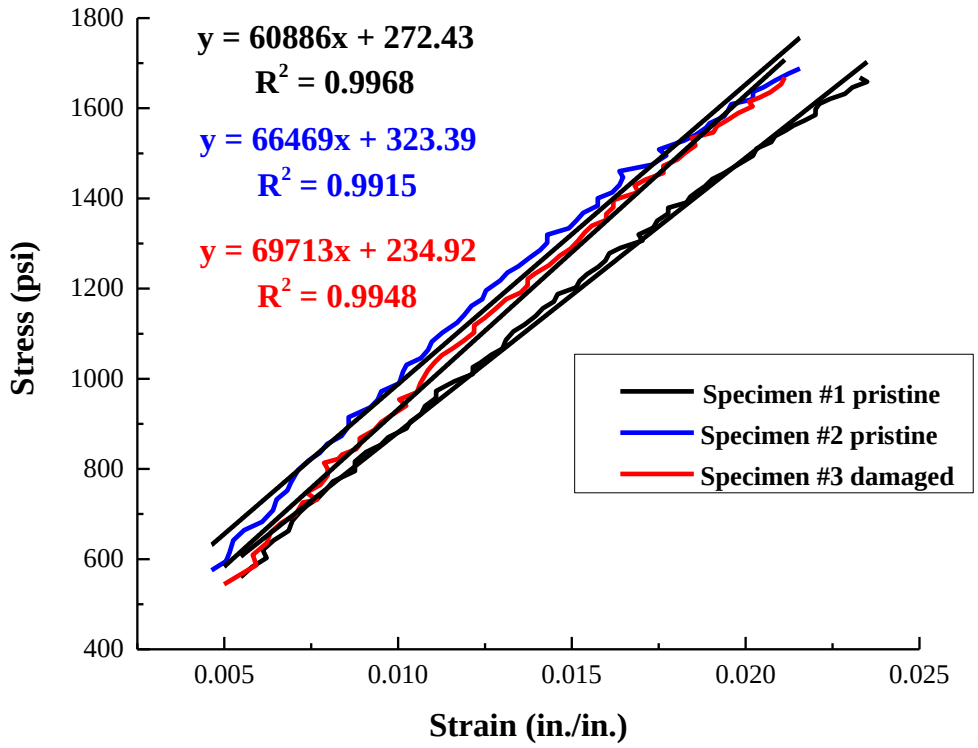

Figure 24. Tensile modulus for Surlyn®/10wt.% chopped glass fiber blends shot at 50°C.

Shown in Figure 25 is a Surlyn®/25wt.% chopped graphite blends which show an impacted vs. pristine residual value of 312 lbf / 555 lbf = 57%. Due to the inclusion of the relatively brittle graphite fibers, the residual strength is reduced as compared to other formulations.

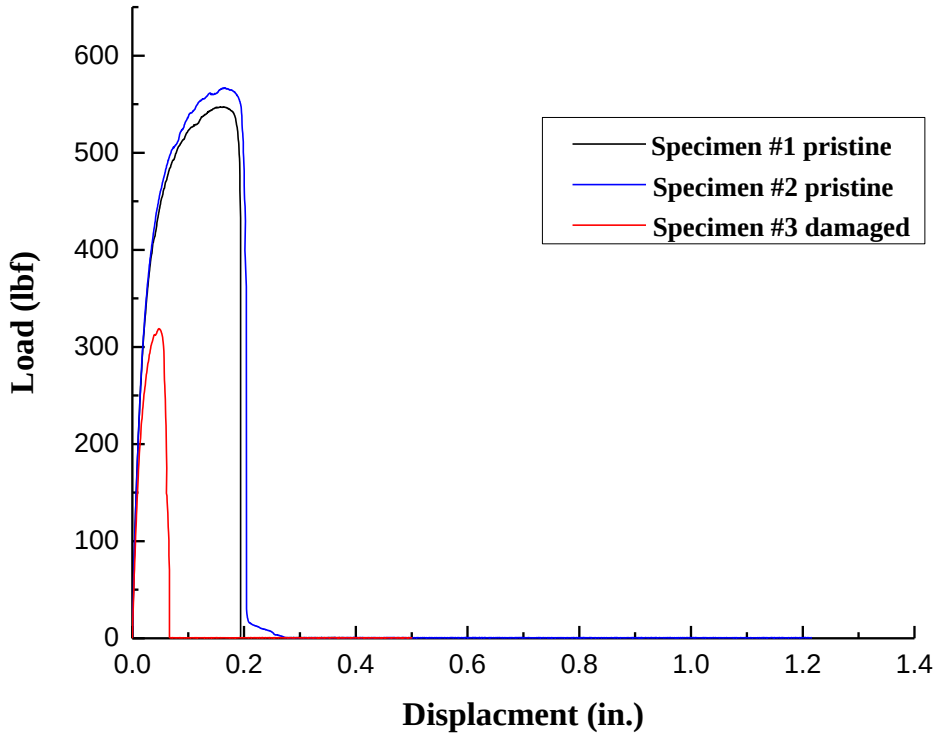

Figure 25. Load displacement curves for non-impacted and impacted Surlyn®/25wt.% chopped graphite fiber blends (shot at 25°C).

Shown in Figure 26 are the modulus calculations for this specimen set. Given that the average modulus of the pristine specimens is about 379,191 psi and that of the impacted specimen is 218,173 psi, a reduction in the modulus of about 44% was produced due to the high fiber content, and matrix material, being dispersed during impact.

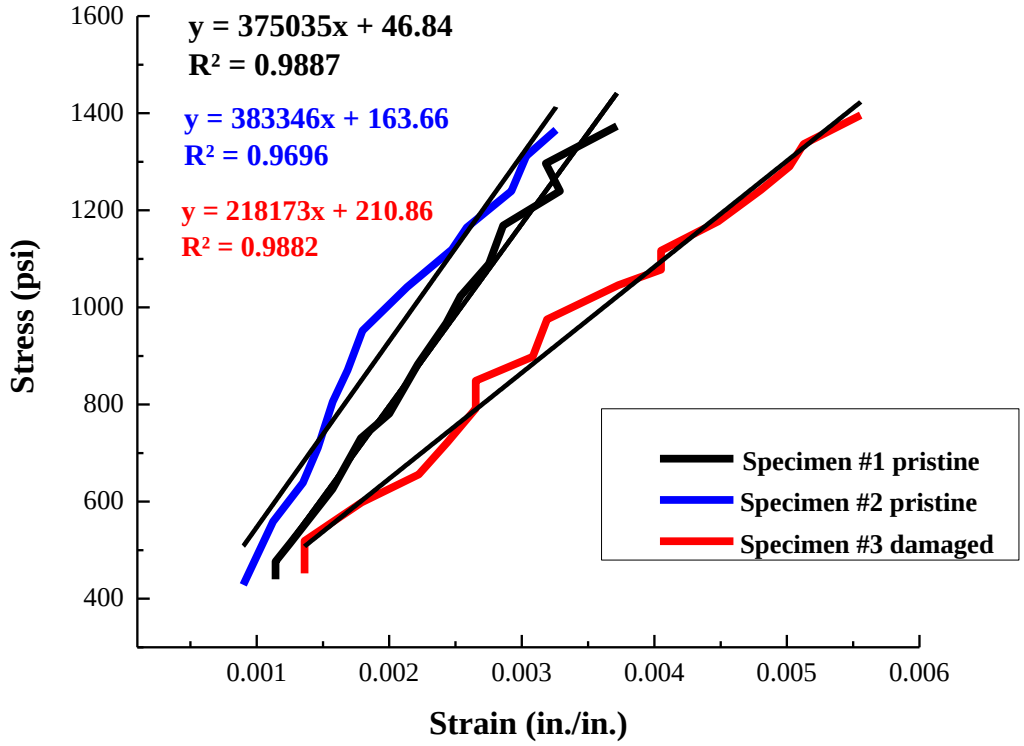

Figure 26. Tensile modulus for Surlyn® /25wt.% chopped graphite fiber blends (shot at 25ºC).

With regards to Figures 27 through Figure 36 one can see that throughout the total range of stroke, no tensile strength was lost, and both the pristine and impacted specimens performed equally well (and hence can be assumed to have retained 100% of their tensile strength over the range of deformation). However, looking at the modulus values, and in particular the initial modulus and how it occurs over a very small, and low load level, it can be immediately recognized that the Affinity® blends exhibit better self-healing behavior as compared to the Surlyn® blends, without reinforcing fibers. The Affinity blends are more of a stand-alone self-healing system, than the Surlyn blends, which look more promising for structural grade fiber/matrix systems.

Shown in Figure 27 is a baseline load vs. displacement test of pure Affinity® EG8200G without any additional blend materials. As shown in the figure, the linear region of response is very small, with almost a constant non-linear response following that section. The maximum load level, through the range of deformation, was only about 45 lbf at a 3.25 inch stroke.

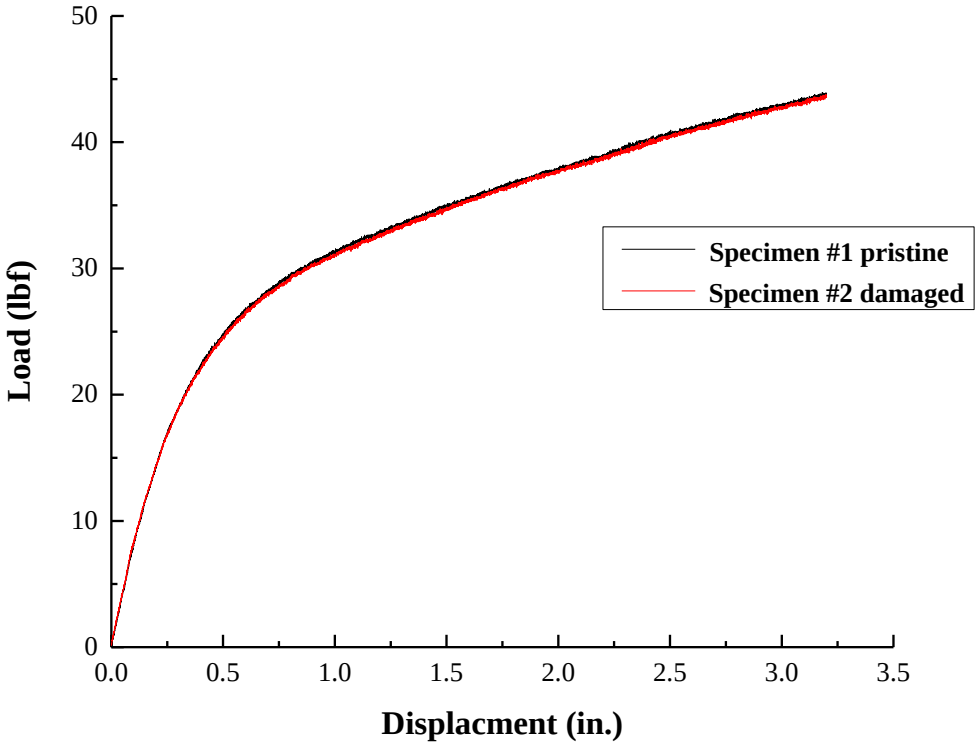

Figure 27. Load displacement curves for non-impacted and impacted Affinity® EG8200G (shot at 25°C).

Shown in Figure 28 is the initial and final modulus calculations for the pure Affinity® EG8200G. Due to the highly non-linear responses for these blends, rather than a tangent modulus method, this approach was selected. As shown, the average initial modulus was about 1,333 psi and the average final modulus was about 81 psi.

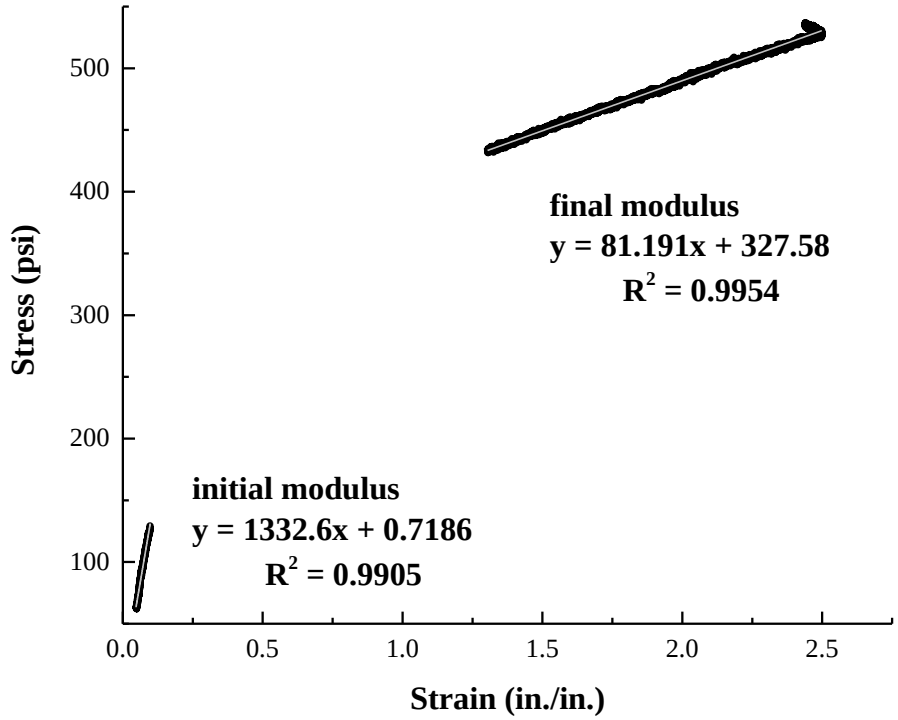

Figure 28. Typical initial and final modulus values for Affinity® EG8200G (shot at 25ºC).

Figure 29 shows the load vs. displacement curve for the Affinity® EG8200G/5wt% PETI-330 (shot at 25ºC) blends. The maximum load is around 35 lbf at a stroke of 3.25 inches. Shown in Figure 30 are the modulus calculations with an average initial modulus of 1,345 psi and an average final modulus value of 31 psi.

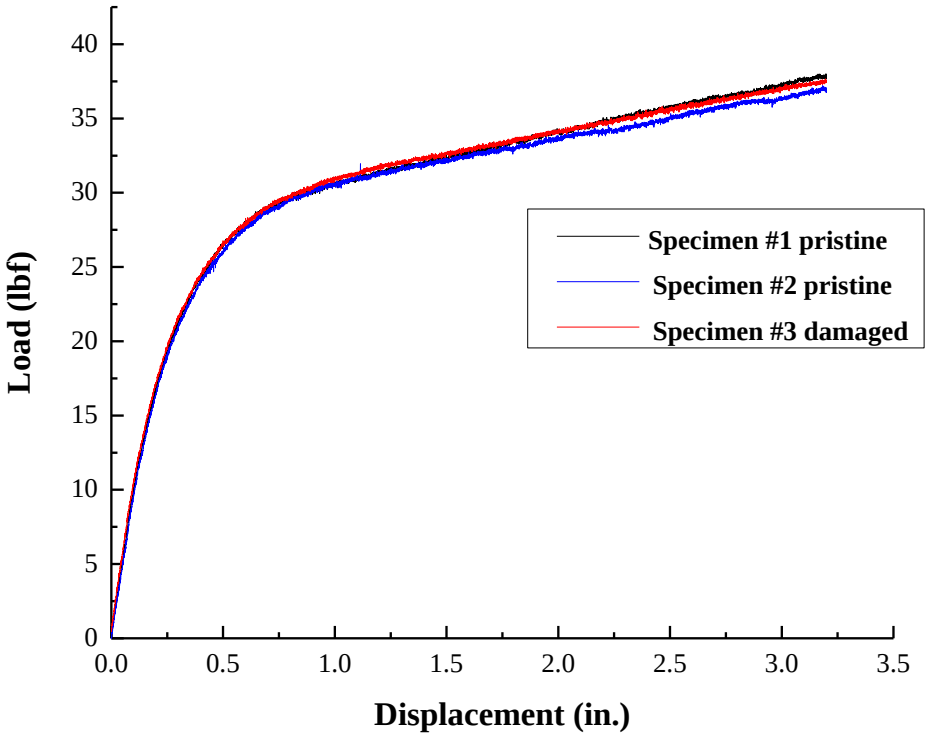

Figure 29. Load displacement curves for pristine and impacted Affinity® EG8200G/5wt.% PETI-330 (shot at 25°C) blends.

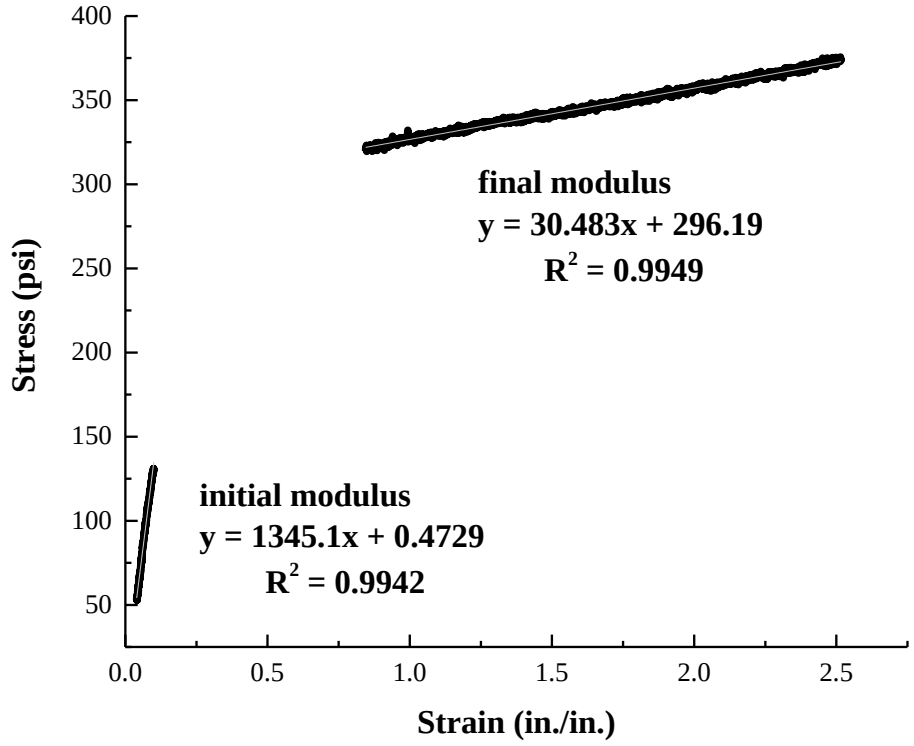

Figure 30. Typical initial and final modulus values for Affinity® with 5wt.% PETI-330 (shot at 25ºC).

Shown in Figure 31 are the Affinity® EG8200G /5wt.% BMI blends (shot at 25ºC and 50ºC) and as shown, the maximum average loads for the 25ºC specimens were about 44 lbf and those of the 50ºC set were at about an average load of 49 lbf. As seen in Figure 32, the average initial modulus for the 25ºC specimens was 1,159 psi and the average final modulus was at 55 psi; for the 50ºC specimens, the average initial modulus was 1,108 psi and the average final modulus was 70 psi.

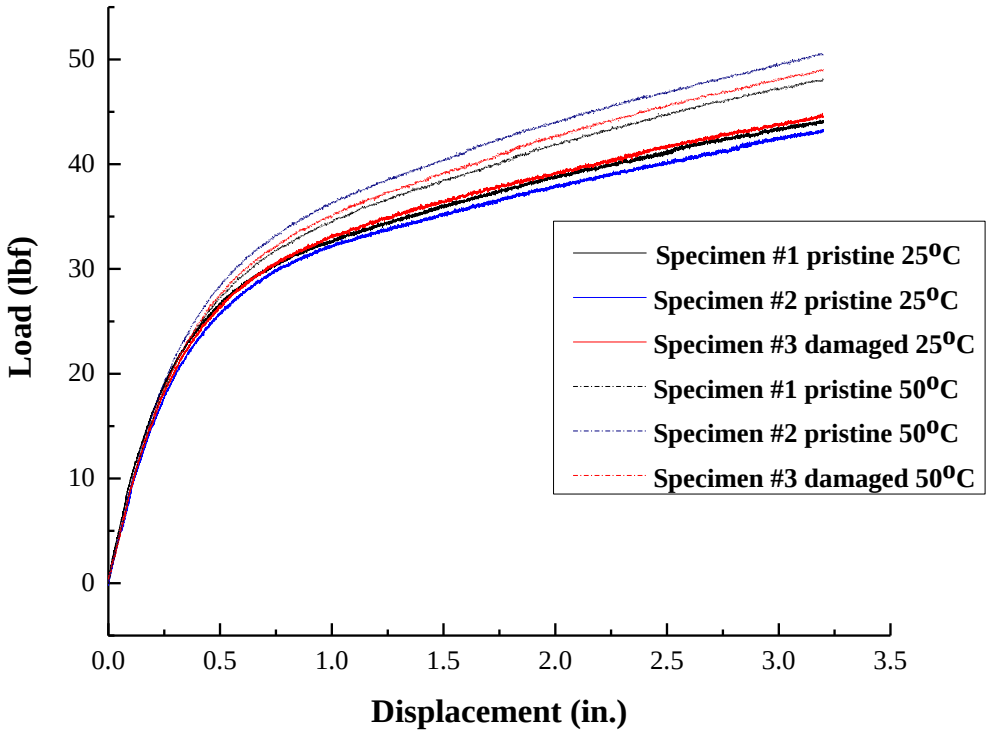

Figure 31. Load displacement curves for pristine and impacted Affinity® EG8200G /5wt.% BMI blends (shot at 25ºC and 50ºC).

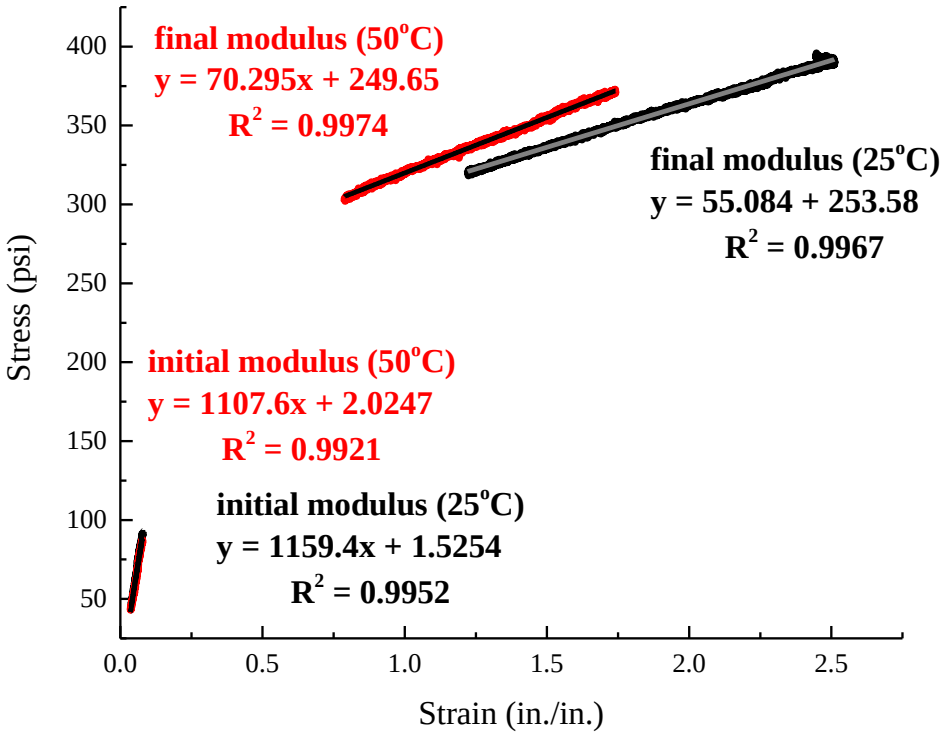

Figure 32. Typical initial and final modulus values for Affinity® with 5wt.% BMI (shot at 25ºC and 50ºC).

Shown in Figure 33 is the load vs. displacement curves for the Affinity® EG8200G /10wt.% Barex 210 IN blends (shot at 25ºC and 50ºC). As shown, the 25ºC specimens had an average maximum load of 44 lbf and those for the 50ºC were at 40 lbf; Figure 34 shows an average initial modulus, for the 25ºC specimens of 1,266 psi and an average final modulus of 42 psi. The 50ºC specimens had an average initial modulus of 1,135 psi and a final average modulus of 45 psi.

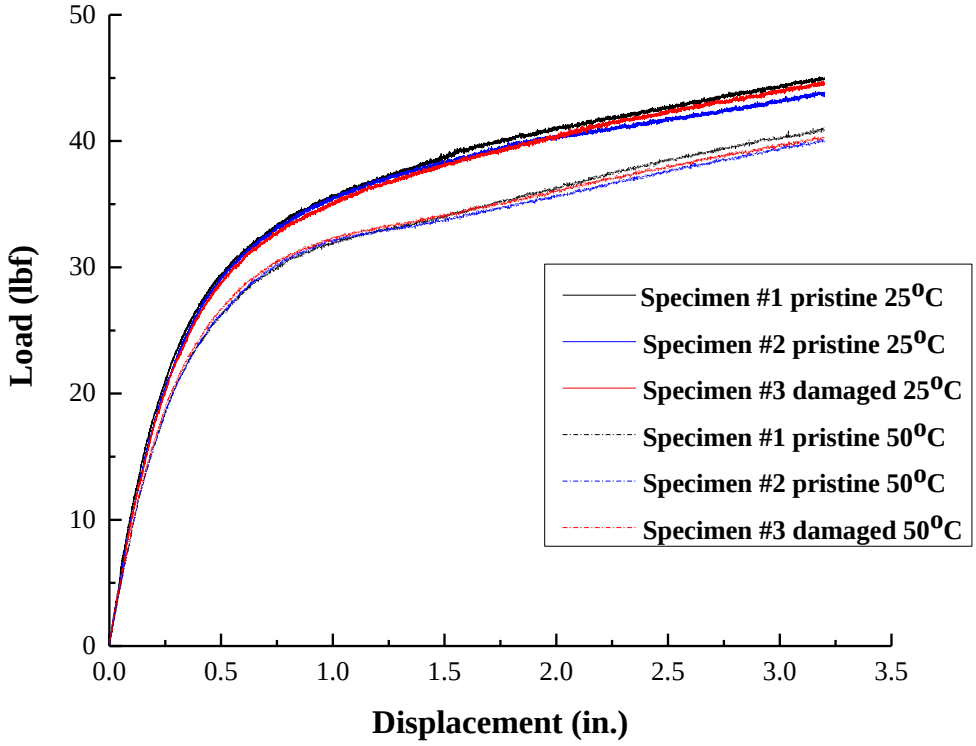

Figure 33. Load displacement curves for non-impacted and impacted Affinity® EG8200G /10wt.% Barex 210 IN blends (shot at 25°C and 50°C).

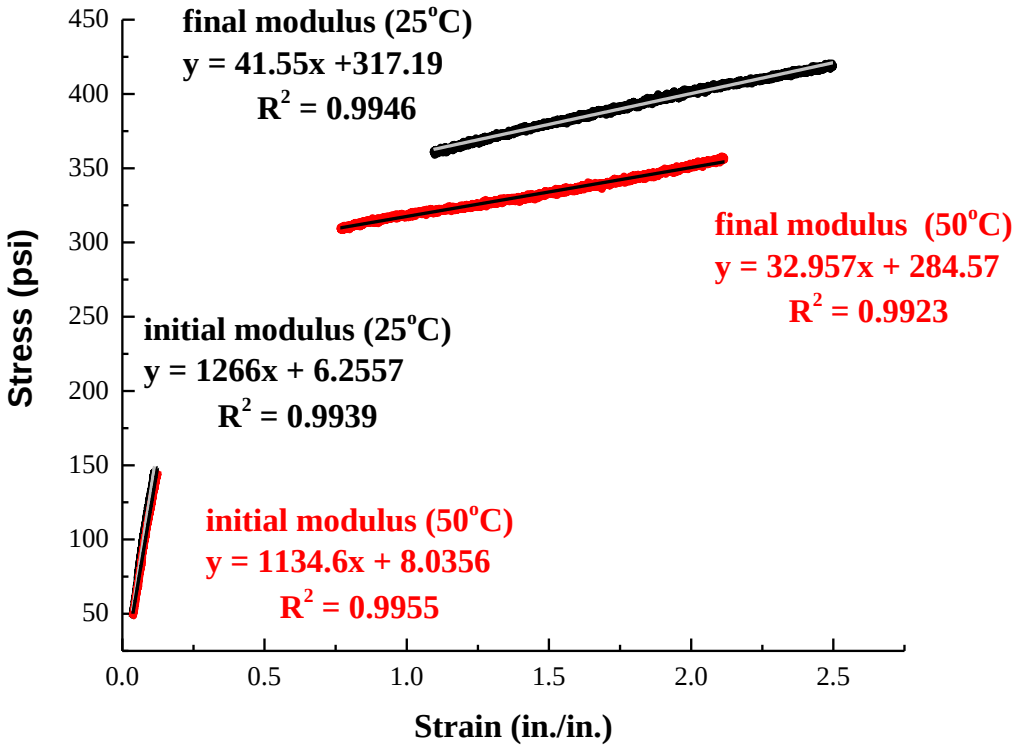

Figure 34. Typical initial and final modulus values for Affinity® with 10wt.% Barex® (shot at 25°C and 50°C).

Shown in Figure 35 are the load vs. displacement curves for the Affinity® EG8200G /5wt.% Barex® 210 IN blends (shot at 25°C and 50°C). For these curves, due to the fact that they lay essentially on top of one another, the overall average maximum load is seen to be about 41 lbf. As shown in Figure 36 the average initial modulus value can be seen to be 1,185 psi, and the average final modulus is 45 psi for the 25°C specimens; for the 50°C specimens, the average initial modulus is 1,029 psi and the average final modulus is 43 psi.

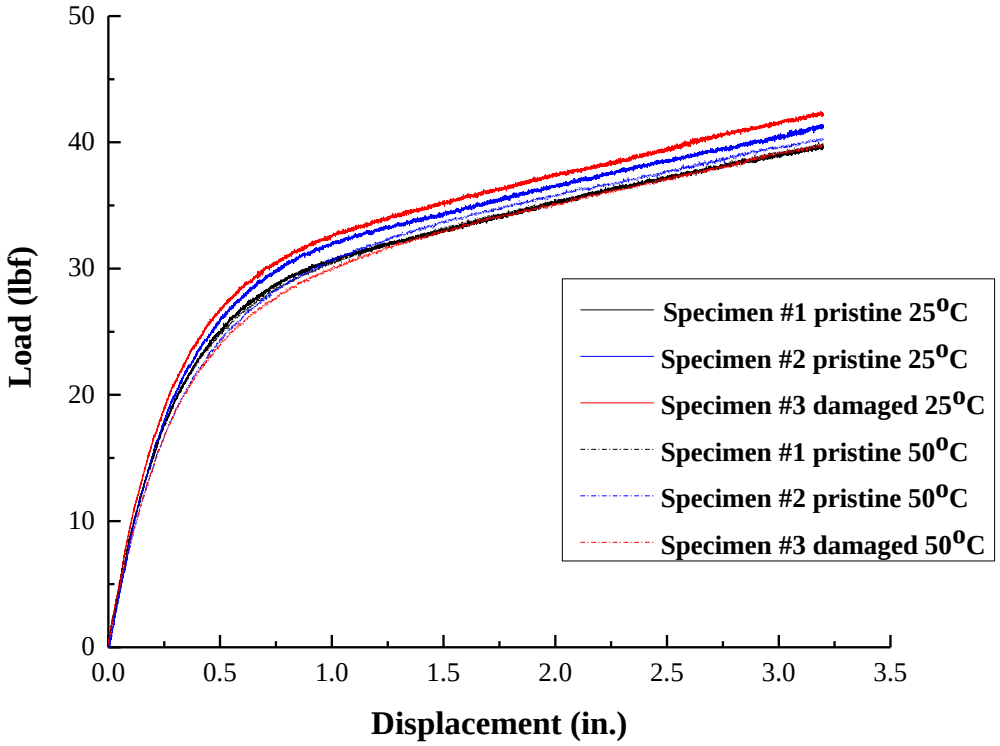

Figure 35. Load displacement curves for non-impacted and impacted Affinity® EG8200G/5wt.% Barex® 210 IN blends (shot at 25°C and 50°C).

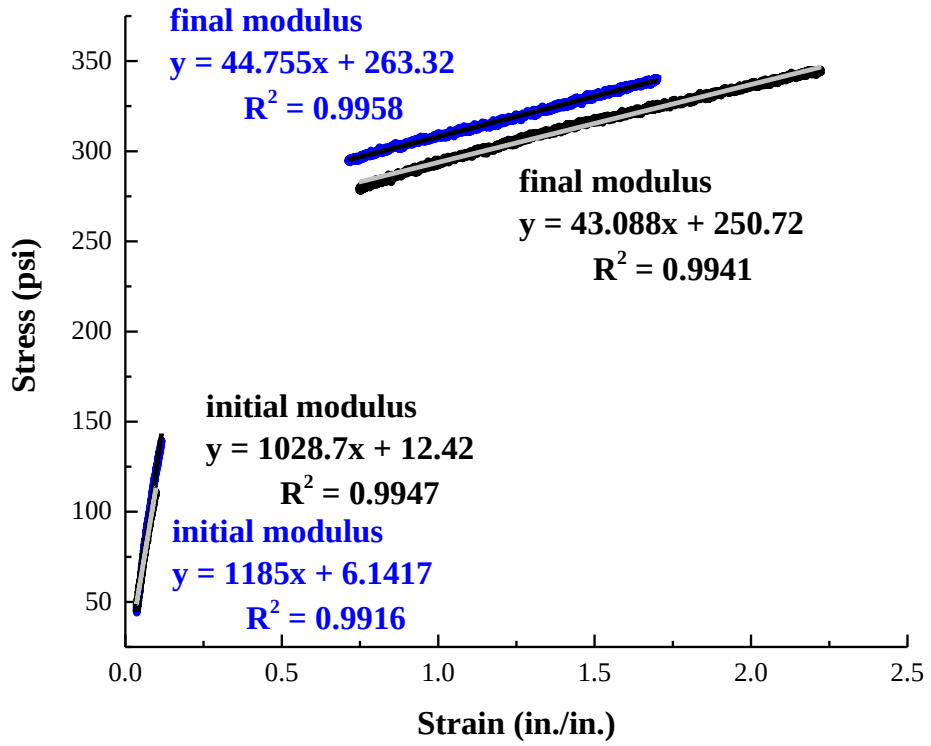

Figure 36. Typical initial and final modulus values for Affinity® with 5wt.% Barex® 210 IN blends (shot at 25ºC and 50ºC).

Summary

As outlined in Table 1 was a listing of the self-healing and high performance polymers along with the engineered polymer blends that were prepared in these studies. Also shown were their respective glass transition temperatures (T_g), melting temperatures (T_m), and thermal decomposition temperatures and whether or not the material healed. Table 2 outlined specific results for the Surlyn® blends which included both chopped glass and graphite fibers, with all of those blends showing self-healing except for the Surlyn®/25wt.% chopped graphite fiber at ca. 50ºC. Also, shown in Table 3 was the TAP and vacuum hold times of the engineered blends. As can be seen in the table, the worst residual strength value is associated with the Surlyn®/25wt.% chopped graphite fiber specimens, shot at ca. 25ºC, but all of the other residual strength values can be seen to be near a minimum of 70% with many blends retaining almost, if not, 100% of their strength over the range of deformation.

The tensile properties of the pristine and impacted blends for all specimens are listed in Tables 4 and 5. The undamaged specimens displayed a typical load-displacement curve whereby after reaching the yield point, the specimen either failed in tension, or did not break before maximum displacement of the test machine was reached. In contrast, many of the damaged specimens broke in tension shortly after reaching the tensile yield point. The Surlyn® based specimens

demonstrated a TAP of at least 70% of the original properties across all ballistic test temperatures (except for the Surlyn®/25wt.% chopped graphite fiber specimens). The Surlyn®/5wt.% PETI-330 processed at 250ºC and shot at ca. 100ºC had a TAP of 80% and the Surlyn®/5wt.% BMI panel shot at ca. 100ºC had a TAP of 83%, which represents the highest residual strength for the Surlyn® based formulations. The Surlyn®/25wt.% chopped graphite fiber formulation demonstrated the lowest TAP for the Surlyn® based blends at 57% of pristine, but had the highest tensile modulus of all blends prepared at 383,346 psi prior to ballistic testing. Although the blend healed, the low TAP is a result of the higher tensile modulus which is not conducive to healing since the more rigid and stiff the material, the more material is lost at impact, resulting in a lower TAP. For comparison, pristine Surlyn® 8940 has a tensile modulus of 40,610 psi and TAP of 70%.

Specimen	Pristine #1 (psi)	Pristine #2 (psi)	Impacted #3* (psi)	E_T (psi)
5wt.% cgf @ 25ºC	n/a	47,875	44,484	46,180
5wt.% cgf @ 50ºC	31,192	37,931	30,180	33,101
10wt.% cgf @ 25ºC	52,755	39,572	38,771	43,699
10wt.% cgf @ 50ºC	60,886	66,469	69,713	65,689
25wt.% cgf @ 25ºC	375,035	383,346	218,173	325,518
5wt.% PETI-330 @ 100ºC	28,705	26,678	26,374	27,252
10wt.% PETI-330 @ 100ºC	35,389	n/a	39,725	37,557
5wt.% BMI @ 100ºC	54,575	39,694	37,267	43,845

* Indicates only one data point.

Table 4. Surlyn® Specimen Tensile Modulus Values.

Specimen	Specimen	E_T Initial (psi)	E_T Final (psi)
Affinity®, 100% @ 25ºC	P#1	1,333	81
5wt.% PETI-330 @ 25ºC	P#1	1,345	31
5wt.% BMI @ 25ºC	P#1	1,159	55
5wt.% BMI @ 50ºC	I#3	1,108	70
10wt.% Barex® @ 25ºC	I#3	1,266	42
10wt.% Barex® @ 50ºC	I#3	1,135	33
5wt.% Barex® @ 25ºC	P#2	1,185	45
5wt.% Barex® @ 100ºC	P#1	1,029	43

Table 5. Affinity® Specimen Tensile Modulus Values.

The mechanical properties of Surlyn® based formulations benefited from the addition of the 5-10% high performance polymeric components and/or chopped fiber inclusions. TAP residual strengths for the Surlyn® blends were higher than pristine Surlyn® with the exception of the

previously mentioned Surlyn®/25wt.% chopped graphite blend which had a 57% residual value; although, Surlyn®/25wt.% chopped graphite blend puncture healed despite having the highest tensile modulus of all Surlyn® based blends. These results suggest that while pristine Surlyn® does not possess the mechanical properties to allow use in structural applications, addition of chopped fibers can yield more desirable properties to make it a candidate for some applications.

For the puncture healing Affinity® blends, the mechanical properties were essentially unchanged (Figures 27-36) by the ballistic event, at a given test temperature. The pristine and damaged specimens displayed very similar load-displacement curves; after reaching a yield point, the specimens continued to stretch in tension until maximum stroke displacement was reached. Although the tensile properties for the Affinity® based specimens were low, TAP residual strengths of 97% and greater were retained.

Conclusions

A series of novel blends comprised of commercially available puncture healing polymers and engineering polymers were fabricated, characterized, and tested for hypervelocity impact behavior. Characterization using DSC, TGA, high speed video, high speed thermography, and an Instron Microtester, were used to confirm material properties of the engineered blends. Residual strengths of panels after ballistic penetration were calculated from tensile strengths and self-healing efficiency was validated by a secondary pressure test; tensile moduli were also calculated for the blends. Concluding statements regarding mechanical data can only be generalized due to the limited number of specimens for each formulation. The puncture healing engineered blends showed improved thermo-mechanical properties over the initial self-healing polymers which were prepared. Affinity® based blends retained nearly 100% of their tensile strength over the range of deformation, but with a very low final modulus value, denoting a non-linear material response. However, tensile modulus values indicate that while Affinity® blends healed better than Surlyn® blends, the latter performed better in fiber reinforced composite form. This work demonstrated a viable approach towards the modification of polymer systems that possess the ability to puncture, and heal, after hypervelocity impacts, based on dynamic molecular properties imparted from their inherent chemical constitution.

References

1. (a). "*Space Transportation costs: Trends in Price Per Pound to Orbit*," **Sept. 6, 2002** issue, 1990-2000. (b). http://swfound.org/media/93632/SSI_Full Report_2012.pdf.
2. Christiansen, E.L., "*Meteoroid/Debris Shielding*," NASA TP-2003-210788, **August 2003**.
3. Whipple, Fred L., "*Meteorites and Space Travel*," Astronomical Journal, **1947**, 52: 131.
4. Fuente, H. de la., Rabion, J.L., Spexarth, G.R., Valle, G.D., "*Transhsb.: NASA's Large-Scale Inflatable Spacecraft*," Proceedings of the AIAA Space Inflatables Forum; Structures, Structural Dynamics, and Materials Conference, **April 3-6, 2000**, paper # 2000-1822.
5. Wool, R.P., Polymer Interfaces: *Structure and Strength* (Hanser/Gardner, Munich, **1995**).
6. White, S.R., Sotto, N.R., Geubelle, P.H., Moore, J.S., Kessler, M.R., Sriram, S.R., Brown, E.N., Viswanathan, S., *Nature,* **2001**, 409, 794-797.
7. Dry, C., McMillan W., *Smart Mater. Struct.*, **1996**, 5(3), 297-300.
8. Pang, J.W., Bond, I.P., *Composites Part A: Applied Science and Manufacturing*, **2005**, 36(2), 183-188.

9. Pang, J.W., Bond, I.P., *Composites Science and Technology*, **2005**, 65 (11-12), 1791-1799.
10. White, S.R, Sottos, N.R., K. Toohey, K., Lewis, J., Moore, J., *Nature*, 6, **2007**, 581-584.
11. John, M., Li, G., *Smart Mater. Struct.*, **2010**, 19, 075013-075024.
12. Nji, J., Li, G., *Smart Mater. Struct.*, **2010**, 19, 035007-035015.
13. Meure, S., Furman, S., Khor, S., *Macromol. Mater. Eng*., **2010**, 295, 420-424.
14. Chen, X., Wudl, F., Mal, A.J., Shen, H., Nutt, S.R., *Macromolecules*, **2003**, 34, 1902.
15. Chen, X., Dam, M., Ono, K., Mal, A., Shen, H., Nutt, S.R., Sheran, K., Wudl, F., *Science*, **2002**, 295, 1698-1702.
16. Wojtecki, R., Meador, M., Rowan, S.J., *Nature Materials*, **2011**, 10, 14-27.
17. Cheng, S., Mather, B. D., Long, T. E., *Polymer Preprints*, **2008**, 49(1), 978-979.
18. Cordier, P., Tournilhac, F., Soulie´-Ziakovic, C., Leibler, L., *Nature*, **2008**, 451, 977-980.
19. Canadell, J., Goossens, H., Klumperman, B., *Macromolecules*, **2011**, 44, 2536-2541.
20. Burnworth, M., Tang, L., Kumpfer, J., Duncan, A., Beyer, F., Fiore, G., Rowan, S., Weder, C., *Nature*, **2011**, 472, 334.
21. Deng, G., Tang, C., Li, F., Jiang, H., Chen, Y., *Macromolecules*, **2010**, 43, 1191-1194.
22. Smith, J., "*An Assessment of Self-Healing Fiber Reinforced Composites*," NASA/TM–2012-217325, **2011**.
23. Lantman, C.W., Macknight, W.J., *Annual Rev. Mat*., **1989**, 19, 295.
24. Hird, B., Eisenberg, A., *Macromolecules*, **1992**, 25, 6466.
25. Fall, R., M.S. thesis entitled, "*Puncture reversal of ethylene ionomers – Mechanistic Studies*" submitted to the faculty of Virginia Polytechnic Institute and State University, Blacksburg, VA **2001**.
26. Kalista, S., M.S. thesis entitled, "*Self-healing Thermoplastic Poly(Ethylene-co-Methacrylic Acid) Copolymers Following Projectile Puncture*" submitted to the faculty of Virginia Polytechnic Institute and State University, Blacksburg, VA **2003**.
27. (a). Varley, R.J., van der Zwaag, S., *Acta Materialia*, **2008**, 56, 5737–5750; (b). Gordon, K.; Penner, R.; Bogert, P.; Yost, W. T.; Siochi, E. *Abstr. Pap. Am. Chem. Soc*., **2011**, 242; (c). Grimsley, B., Gordon, K., Czabaj, M., Cano, R., Siochi. M., "*Processing and Damage Tolerance of Continous Carbon Fiber Composites containing Puncture Self-healing Thermoplastic Matrix*," Proceedings of the Society of Materials Process Engineering Conference (SAMPE) held in Baltimore, MD (**May 21-24, 2012**).
28. Varley, R.J., van der Zwaag, S., *Polym. Int.*, **2010**, 59, 1031–1038.
29. Klein, D., United States Patent #8,063,171, "*Self-healing polymers*," **Nov. 22, 2011**.
30. Gordon, K., Bogert, P., Howell, P., Burke, E., Cramer, E., Yost, W.T., and Siochi, E., "*Ballistic Puncture Self-healing Polymeric Materials,"* submitted as NASA/TM (April **2015**).
31. ASTM D638-10, "*Standard Test Method for Tensile Properties of Plastics*," ASTM International, West Conshohocken, PA, **2010**, DOI: 10.1520/D0638-10, www.astm.org.

REPORT DOCUMENTATION PAGE

Form Approved
OMB No. 0704-0188

1. REPORT DATE *(DD-MM-YYYY)*	2. REPORT TYPE	3. DATES COVERED *(From - To)*
01- 03 - 2016	Technical Memorandum	

4. TITLE AND SUBTITLE

Engineering Polymer Blends for Impact Damage Mitigation

5a. CONTRACT NUMBER

5b. GRANT NUMBER

5c. PROGRAM ELEMENT NUMBER

6. AUTHOR(S)

Gordon, Keith L.; Smith, Russell W.; Working, Dennis C.; Siochi, Emilie J.

5d. PROJECT NUMBER

5e. TASK NUMBER

5f. WORK UNIT NUMBER

247926.06.04

7. PERFORMING ORGANIZATION NAME(S) AND ADDRESS(ES)

NASA Langley Research Center
Hampton, VA 23681-2199

8. PERFORMING ORGANIZATION REPORT NUMBER

L-20549

9. SPONSORING/MONITORING AGENCY NAME(S) AND ADDRESS(ES)

National Aeronautics and Space Administration
Washington, DC 20546-0001

10. SPONSOR/MONITOR'S ACRONYM(S)

NASA

11. SPONSOR/MONITOR'S REPORT NUMBER(S)

NASA-TM-2016-219002

12. DISTRIBUTION/AVAILABILITY STATEMENT

Unclassified - Unlimited
Subject Category 23
Availability: NASA STI Program (757) 864-9658

13. SUPPLEMENTARY NOTES

14. ABSTRACT

Structures containing polymers such as DuPont's Surlyn® 8940, demonstrate puncture healing when impacted by a 9 mm projectile traveling from speeds near 300 m/sec (1,100 ft/sec) to hypervelocity impacts in the micrometeoroid velocity range of 5 km/sec (16,000 ft/sec). Surlyn® 8940 puncture heals over a temperature range of -30oC to +70oC and shows potential for use in pressurized vessels subject to impact damage. However, such polymers are difficult to process and limited in applicability due to their low thermal stability, poor chemical resistance and overall poor mechanical properties. In this work, several puncture healing engineered melt formulations were developed. Moldings of melt blend formulations were impacted with a 5.56 mm projectile with a nominal velocity of 945 m/sec (3,100 ft/sec) at 25oC, 50oC and 100oC, depending upon the specific blend being investigated. Self-healing tendencies were determined using surface vacuum pressure tests and tensile tests after penetration using tensile dog-bone specimens (ASTM D 638-10). For the characterization of tensile properties both pristine and impacted specimens were tested to obtain tensile modulus, yield stress and tensile strength, where possible. Experimental results demonstrate a range of new puncture healing blends which mitigate damage in the ballistic velocity regime.

15. SUBJECT TERMS

High performance polymers; Melt blends; Self-healing polymers

16. SECURITY CLASSIFICATION OF:			17. LIMITATION OF ABSTRACT	18. NUMBER OF PAGES	19a. NAME OF RESPONSIBLE PERSON
a. REPORT	b. ABSTRACT	c. THIS PAGE			STI Help Desk (email: help@sti.nasa.gov)
					19b. TELEPHONE NUMBER *(Include area code)*
U	U	U	UU	46	(757) 864-9658